Winter 2020

Using Stable Isotopes to Determine Dominant Methane Production Pathways of Thaw Ponds in a Subarctic Peatland

Kathryn Ann Bennett
University of New Hampshire, Durham

Using Stable Isotopes to Determine Dominant Methane Production Pathways of Thaw Ponds in a Subarctic Peatland

By

Kathryn A. Bennett

B.Sc. Environmental Science: Ecosystems and Sustainability, University of New Hampshire, 2019

THESIS

Submitted to the University of New Hampshire

In Partial Fulfillment of

The Requirements for the Degree of

Master of Science

In

Earth Sciences: Geochemical Systems Specialization

December 2020

This thesis was examined and approved in partial fulfillment of the requirements for the degree of Master in Earth Science by:

Thesis Director, Ruth Varner, Professor of Biogeochemistry, Department of Earth Sciences and Earth Systems Research Center

Julia Bryce, Professor of Geochemistry, Department of Earth Sciences

Jessica Ernakovich, Assistant Professor of Microbial Ecology, Department of Natural Resources and the Environment

On November 13, 2020

Approval signatures are on file with the University of New Hampshire Graduate School.

ACKNOWLEDGEMENTS

First, I would like to thank my advisor, Dr. Ruth K. Varner, for her incredible mentorship throughout my time at UNH and for introducing me to the beauty of Stordalen Mire. Thank you to my committee members, Dr. Jessica Ernakovich and Dr. Julie Bryce for their invaluable mentorship and guidance. I am fortunate to be surrounded by such inspirational female scientists and hope to one day be at least half the role model you have all been to me. I would also like to thank Dr. Sophia Burke for her mentorship and contributions to data collection and interpretation, and Ms. Clarice Perryman for her contributions to data collection and her unwavering support as a friend and lab-mate. I would also like to acknowledge the contributions to this project made by Dr. Carmody McCalley, Ms. Jessica DelGreco, Dr. Michael Palace, Dr. Jeff Chanton, Dr. Joanne Shorter, and Dr. Patrick Crill. Thank you to the members of the Trace Gas Biogeochemistry Lab for their continued support and feedback, especially Ms. Apryl Perry for her assistance with lab work. Thank you to Ms. Stacey Doherty, Ms. Allison Herreid, and Mr. Peter Tansey, and for their support during field work in the form of assistance and comradery, and to Ms. Katie Rocci for her contributions to data collection. Thank you to the Abisko Scientific Research Station and the many friends I made there for their hospitality and assistance during summer field campaigns. Finally, thank you to my family and friends for supporting me no matter where in the world my research takes me. Without their encouragement I may never have traveled to Sweden for the first time to begin this journey.

This project was supported by funding from the University of New Hampshire (UNH) Graduate School Summer Teaching Assistant Fellowship, Teaching Assistantships from the UNH Earth Science Department, the UNH Department of Earth Science summer research fund, the UNH Hamel Center for Undergraduate Research, the UNH Graduate School travel fund, the

New Hampshire Space Grant, and grants to Dr. Ruth Varner: US National Science Foundation's REU: Northern Ecosystems Research for Undergraduates (EAR#1063037), the US National Science Foundation's (NSF) MacroSystems Biology grant (EF-1241937), the US Department of Energy Office of Biological and Environmental Research under the Genomic Science program (Awards DE-SC0004632, DE-SC0010580, DE-SC0016440), and the National Aeronautics and Space Administration's Archaea to the Atmosphere award (NASA #NNX17AK10G). The data associated with this work are stored on the data repository site of the ISOGENIE project and can be found online (https://isogenie-db.asc.ohio-state.edu/datasources#fluxes).

TABLE OF CONTENTS

LIST OF TABLES

LIST OF FIGURES

ABSTRACT

Arctic and subarctic ecosystems are currently warming faster than any other region of the globe, accelerating seasonal permafrost thaw. As thaw progresses, small water bodies can form due to slumping of the peatland surface. These ponds emit methane (CH_4), a strong, radiatively important trace gas, predominantly through ebullition (bubbling). Two different types of methanogenic Archaea present in these systems produce CH_4 through their respective production pathways: acetoclastic and hydrogenotrophic methanogenesis. The acetoclastic pathway forms CH_4 using CH_3COOH, an organic carbon (C) source while hydrogenotrophic methanogenesis uses CO_2, an inorganic C source. Stable isotopes can be used to characterize the relative contribution of these two pathways in overall CH_4 production and to better constrain the global CH_4 budget and improve modeling of future emission scenarios.

We used stable isotopes, carbon-13 (^{13}C) of CH_4 and CO_2, deuterium (D) of CH_4, and calculated apparent fractionation factors to determine the relative contribution of acetoclastic versus hydrogenotrophic pathways of methanogenesis in thaw ponds in a subarctic peatland located in the discontinuous permafrost region of northern Sweden. Isotopic analysis was performed on porewater samples (n = 310) and gas captured from ebullition (n = 177). Samples were collected from nine ponds over seven years (2012 to 2019) during the ice-free months (June to September). We tested important physical attributes of the ponds that were related to their formation and CH_4 production pathways. Results indicated that $\delta^{13}C$-CH_4 of ebullition (-86.3‰ to -49.2‰) and porewater (98.2‰ to -42.9‰) and the inferred contribution of hydrogenotrophic vs. acetoclastic methanogenesis differed significantly between certain ponds and pond types. Over the course of this study dissolved and ebullitive $\delta^{13}C$-CH_4 remained relatively constant between years but varied significantly between months. Alternatively, δD-CH_4 of ebullition (-

397.0‰ to -199.4‰) and porewater (-383.4‰ to -184.8‰) did not differ between sampling years or months.

Pond types that are partially thawed and have a lower daily CH_4 ebullitive flux appear to have a higher relative contribution of hydrogenotrophic methanogenesis while types that are partially or fully thawed and have a higher daily CH_4 ebullitive flux appear to have a higher contribution of acetoclastic methanogenesis relative to other pond types. Differences in CH_4 isotopic composition between pond types indicates that shifts in isotopic emissions could occur as thaw progresses in northern permafrost ecosystems. While we did observe expansion of ponds and landscape slumping at Stordalen Mire over our 7-year study, a strong trend in isotope signal was not observed likely due to the high interannual variability. This unique multi-year study characterized $\delta^{13}C$-CH_4 and δD-CH_4 values for ebullition and porewater from open-water thaw ponds providing valuable data to constrain the global CH_4 budget and improve modeling of the contribution of these systems to emissions now and in the future.

I. INTRODUCTION

Artic and sub-Arctic ecosystems are currently warming faster than any other region of the planet causing the thaw of permanently frozen soil, or permafrost. Permafrost thaw can manifest as ground slumping and collapse, forming ponds across the landscape that become important sources of methane (CH_4) to the atmosphere as methanogens access newly available C (Burke et al., 2019; Kuhn et al., 2018; Negandhi et al., 2013; Olsen et al., 2011). This production of CH_4, a radiatively important trace gas estimated to be 32 times stronger than carbon dioxide (CO_2) on a 100 year timescale (Holmes et al., 2013), contributes to a positive feedback as CH_4 emissions increase radiative forcing and climate warming that then accelerates permafrost thaw (Schuur et al., 2015; Turetsky et al., 2019).

Methanogenic Archaea are categorized as two different organisms, acetoclasts and hydrogenotrophs that produce CH_4 through unique production pathways: acetoclastic methanogenesis (AM; $CH_3COOH \rightarrow CO_2 + CH_4$) and hydrogenotrophic methanogenesis (HM; $CO_2 + 4H_2 \rightarrow CH_4 + 2H_2O$) respectively. Acetoclastic methanogenesis produces CH_4 using acetate (CH_3COOH), an organic C source while HM uses CO_2. The relative contribution of these two pathways in overall CH_4 production can be inferred using stable isotope analysis of carbon-13 ($\delta^{13}C\text{-}CH_4$) and deuterium ($\delta D\text{-}CH_3D$; Chanton et al., 2006; Chanton et al., 2005; Whiticar, 1999; Whiticar et al., 1986). In addition, the isotopic analysis of dissolved inorganic carbon ($\delta^{13}C\text{-}CO_2$) can be interpreted to indicate the relative contribution of CH_4 production pathways via the calculation of apparent fractionation factor (α_C), a measure of the amount of isotopic separation between the source (CO_2) and produced (CH_4) carbon species (Chanton et al., 2005; Whiticar, 1999; Whiticar et al., 1986). Approximate isotopic values indicating contribution of AM are -40 to -60‰ for $\delta^{13}C$ and -250 to -400‰ for δD while contribution of HM is indicated

by -60 to -110‰ for $\delta^{13}C$ and -170 to -250‰ for δD (Figure 1; Chanton et al., 2006; Hornibrook et al., 1997; Whiticar et al., 1986).

Determining the relative importance of methanogenesis pathways and constraining the isotopic composition of thaw pond CH_4 emissions is essential for improving calculations of the global CH_4 budget, The global budget of CH_4 is generally determined using either "bottom-up" methods that construct process-based models using field measurements or "top-down" methods that construct inverse models using atmospheric measurements, or a combination of the two. Currently, large discrepancies exist between these approaches with the bottom-up global CH_4 emission calculations almost 30% higher than global CH_4 emissions calculated with top-down methods (Saunois et al., 2020). Field-based isotope measurements are an essential tool to improve agreement between these two methods and provide more accurate estimates of CH_4 emissions from notable sources such as changing permafrost ecosystems (McCalley et al., 2014).

The relative contribution of methanogenic pathways is influenced by climate, hydrologic conditions, and vegetation composition (Berger et al., 2018; Chanton, 2005; Prater et al., 2007; Waldron et al., 1999). These properties change as thaw stage advances in northern peatlands, suggesting that change in the contribution of these two methanogenic pathways and a consequent shift in the emission of $\delta^{13}C$-CH_4 occurs with thaw progression (McCalley et al., 2014). Thaw transitions from dry, elevated palsa plateaus to submerged bog, fen, and pond areas have been documented across the Arctic (Johansson et al., 2006; Johnston et al., 2014; Quinton et al., 2011; Vitt et al., 2000) and associated with differences in isotopic composition of CH_4 diffusive fluxes (McCalley et al., 2014). The presence of different vegetation species and CH_4 transport mechanisms occurring in a system also influence CH_4 fluxes and $\delta^{13}C$-CH_4 signature. The three modes of transport for CH_4 gas flux are plant-mediated, bubbling or ebullition, and diffusion

(Chanton, 2005). Sedge plants common in northern wetlands, including *Carex spp*. and *Eriophorum spp.,* are associated with plant-mediated transport through the process of aerenchyma, acting like a straw to carry gas up through the plant stem and contributing to higher gas efflux (Chanton, 2005; Greenup et al., 2000; Noyce et al., 2014). Methane transported by aerenchyma experiences more fractionation due to oxidation in the rooting zone or rhizosphere. This fractionation enriches the $\delta^{13}C$, making it less negative than the $\delta^{13}C$ unaffected by this process (Chanton, 2005). Ebullition is a more rapid process and does not result is isotopic fractionation, making it a reliable sampling method to infer sediment methane dynamics (Chanton & Martens, 1988) and is often the dominant method of transport from aquatic sediments (Bastviken et al., 2011; Walter et al., 2007). The production and presence of sedge plant species, especially *Carex spp*., drives the relative contribution of acetoclastic versus hydrogenotrophic methanogenesis pathways towards higher contribution of acetoclastic methanogenesis (Bellisario et al., 1999; Prater et al., 2007).

Ebullitive emissions from northern lakes and ponds are a significant source of CH_4 to the atmosphere (Anthony et al., 2020; Burke et al., 2019; Wik et al., 2013) but are not often measured over extended periods of time (Wik et al., 2016). Measurements of the isotopic composition of these ebullitive emissions is even more rare, presenting a gap in scientific understanding of the interannual and seasonal variation of these emissions. Recent data suggests that the relative contribution of CH_4 production pathway does not shift seasonally as indicated by minimal change in $\delta^{13}C$-CH_4 and changes in δD-CH_4 that could be explained by the influence of evaporation documented on a monthly timescale from ebullitive flux measurements (Jansen et al., 2019; Wik et al., 2020). Consistent relative contribution of CH_4 production pathways across months has also been documented in diffusive flux and dissolved CH_4 measurements (McCalley

et al., 2014). Directional change across consecutive years in isotopic composition of CH_4 ebullitive or diffusive flux from thaw-formed lakes or ponds that would reflect a shift in contribution of methanogenesis pathways has not previously been documented (Negandhi et al., 2013; Townsend-Small et al., 2017). Over a period of three years, $\delta^{13}C$ and δD of dissolved methane ranges were found to narrow after a wetting event in sphagnum and sedge dominated wet areas in northeast Siberia suggesting that relative contribution of methanogenesis pathways could shift in response to changes is climatic conditions in permafrost wetlands (Shingubara et al., 2019). Currently, no studies exist that measure $\delta^{13}C$ of CH_4 flux from thaw-formed ponds for period of longer than three years (Blodau et al., 2008; Knoblauch et al., 2015; Nakagawa et al., 2002; Negandhi et al., 2013), making it difficult to determine whether contributions of methanogenesis pathways shifts within ponds in response to increased thaw. Changes in hydrology and vegetation that occur on decadal scales as a result of permafrost thaw (Johansson et al., 2006) could cause shifts in the relative contribution of methanogenesis pathways over a multi-year period in thaw ponds that has not yet been documented by previous short-lived studies.

Thaw ponds at Stordalen Mire in Abisko, Sweden have been categorized into four types based on differences in their daily ebullitive CH_4 flux. These types also vary in their physical characteristics and provide a spatial representation of varying thaw stage (Burke et al., 2019)Extensive pre-existing data from Burke et al., (2019) provides a unique opportunity to examine differences in isotopic composition of dissolved and emitted CH_4 that occur in different pond types and draw conclusions about the relationship between pond CH_4 flux, physical characteristics, and relative contribution of methanogenesis pathways.

The objective of this study is to determine dominant methane production pathways of thaw ponds in a subarctic peatland complex over a multi-year period using stable isotopes ($\delta^{13}C$-CH_4, δD-CH_4, and $\delta^{13}C$-CO_2). We measured $\delta^{13}C$-CH_4 and δD-CH_4 of ebullition and $\delta^{13}C$-CH_4, δD-CH_4, and $\delta^{13}C$-CO_2 of pond sediment porewater from ponds over a period of seven years during the growing season. We hypothesize that (1) $\delta^{13}C$-CH_4 and δD-CH_4 will vary significantly between individual ponds and pond types established by Burke et al. (2019) indicating a difference in the relative contribution of CH_4 production pathways between pond types with more "bog-like" pond in Types 1-3 having more relative contribution of HM and "fen-like" Type 3 ponds having more relative contribution of AM, and (2) we expect to see no significant difference in isotopic signatures of $\delta^{13}C$-CH_4 and δD-CH_4 from ebullition and porewater on a monthly timescale or between years over the duration of this study (7 years) due to the lack of seasonal variation previously documented in isotopic composition of dissolved and emitted CH_4 and the decadal timescale of environmental changes in response to permafrost thaw.

II. METHODS

II. 1. SITE DESCRIPTION

Nine thaw ponds were sampled at Stordalen Mire (68°21′N 18°49′E), a peatland located in the discontinuous permafrost region in Abisko, Sweden (Figure 1). This sub-Arctic ecosystem has a mean annual temperature of 0.6°C and a mean annual precipitation of 300mm (Callaghan et al., 2010). Landcover types include permafrost palsas, *Sphagnum spp*. bogs, shallow lakes, fens, and thaw ponds. A large body of literature including decadal measurements of methane emissions and extensive unmanned aerial system imagery documenting vegetation changes at the Stordalen Mire make it an ideal location to study long-term changes (Johansson et al., 2006; Palace et al., 2018; Svensson et al., 1999).

The pond sites for this study were selected based on their boardwalk proximity and accessibility. The ebullitive CH_4 flux from each pond has been previously measured over a four year period (2012 to 2015) by Burke et al., (2019). Thorough descriptions of these ponds and associated flux measurements can be found in Burke et al., (2019) and are summarized here. The seven ponds included in the study were categorized into four types by significant differences in the ebullitive CH_4 flux that coincided with differences in their physical characteristics, including thaw stage. Type 1 ponds were the lowest emitting (median 0.0 mg CH_4 m^{-2} day^{-1}), located on intact palsa plateaus, the shallowest ponds in the study, hydrologically isolated, and had a relatively low amount of sedge vegetation and high amounts of *Sphagnum spp.* present. Type 2 ponds emitted the next lowest amount of CH_4 (medians: 4.5 and 3.6 mg CH_4 m^{-2} day^{-1}), were surrounded by a combination of intact and collapsing palsas, were deeper than Type 1 ponds, hydrologically isolated, and had increased presence of sedge vegetation relative to Type 1 and contained floating *Sphagnum spp.*. Type 3 ponds emitted the highest amount of CH_4 (medians: 53.4 and 40.9 mg CH_4 m^{-2} day^{-1}), were surrounded by intact and collapsing palsas, were some of the deepest ponds in the study, hydrologically isolated, and had some floating *Sphagnum spp.* with sedge vegetation present along pond edges. Type 4 ponds emitted the second highest amount of CH_4 (medians: 6.4 and 11.7 mg CH_4 m^{-2} day^{-1}), were connected to surrounding fully-thawed fen areas, not hydrologically isolated, and had relatively high coverage of sedge vegetation and no floating *Sphagnum spp.* (Burke et al., 2019).

II. 2. EBULLITION SAMPLING

Ebullition (bubble) samples were collected from the eight of the nine study ponds during the growing season (May – September) from 2012-2019; no samples were collected in 2013 and 2015 (Table 1). Every 1-3 days, samples were collected from floating bubble traps to assess

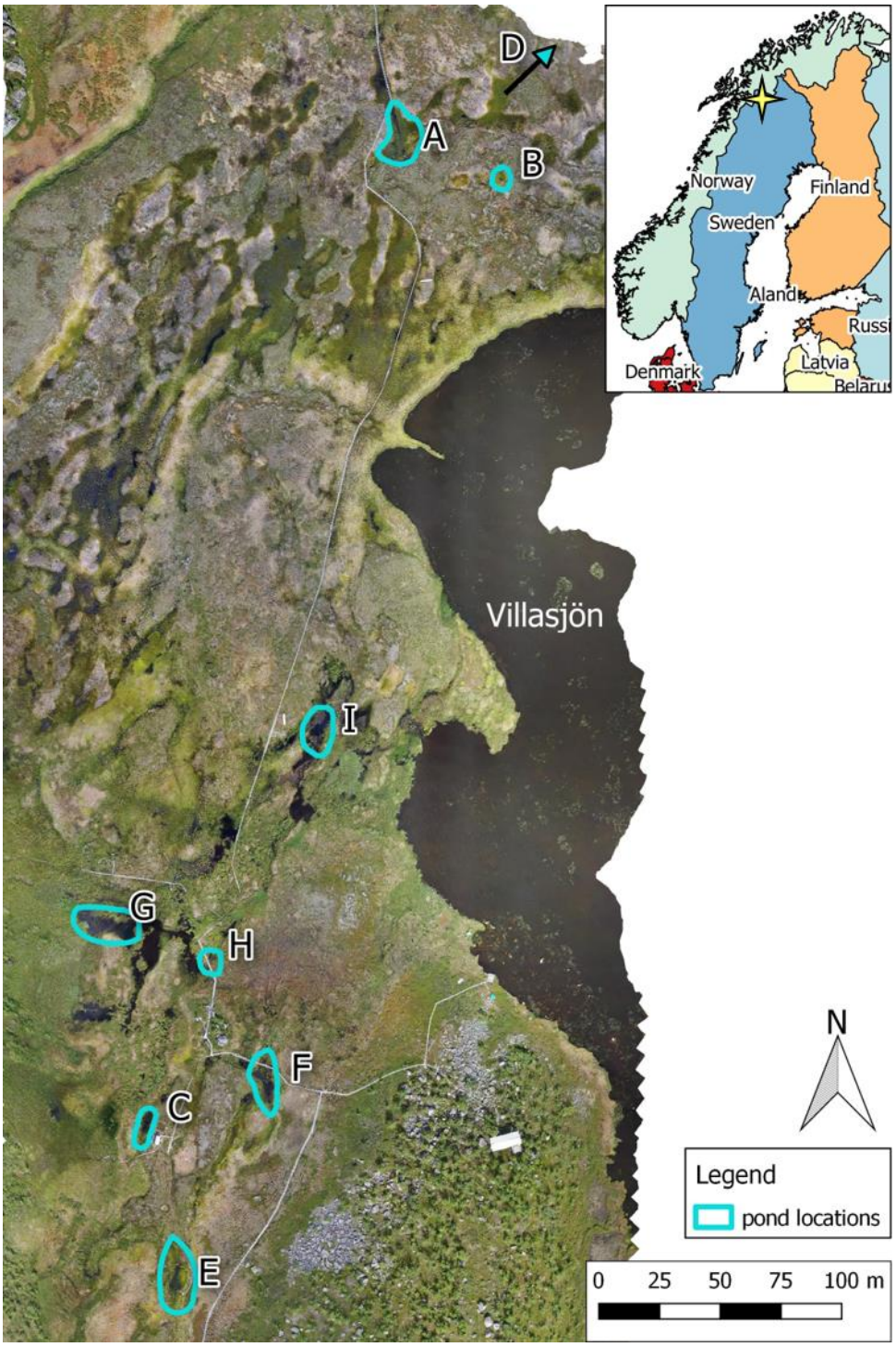

Figure 1. Orthomosaic image of Stordalen Mire in northern Sweden (68°21′N 18°49′E) generated from images collected using an unmanned aerial system at an altitude of 70m on July 22, 2019 courtesy of Dr. Michael Palace. Nine ponds included in this study are labeled with corresponding capital letters. Blue polygons enclose approximate pond locations. Pond D is located out of frame to the northwest of the pictured area as indicated by a blue and black arrow. A yellow star (inset figure) indicates the general location of Stordalen Mire within Sweden. The site map and included polygons were rendered using QGIS (v.2.18.23).

isotopic composition and calculate daily ebullitive flux (Figure 2). Bubble traps were deployed using methodology described in detail by Burke et al. (2019) and were designed similarly to bubble traps used by Wik et al. (2013). Gas samples for isotopic composition were collected from bubble traps using 10-ml polypropylene syringes when the accumulated gas volume in a bubble trap was >5 ml. Samples were then transported to the Abisko Scientific Research Station (ANS) and refrigerated at 2°C for up to 24 hours prior to being stored in 15-ml evacuated glass vials with butyl rubber septa.

II. 3. POREWATER SAMPLING

Porewater dissolved gas samples were collected from eight of the nine ponds once monthly during the growing season adjacent to the bubble trap locations in each pond from 2012-2019 with no samples collected in 2013 and 2015 (Table 1). Samples were obtained using suction with a syringe connected to a 60cm long stainless-steel tube (0.25inch outer diameter) with a perforated end inserted into the peat or sediment to desired depth (Figure 1). Samples (30 ml) were collected at 0, 10, 20, and 40cm depths below the pond bottom. The dissolved gas in the porewater was then equilibrated with 30 ml of room air by shaking the combined air and water for two minutes by

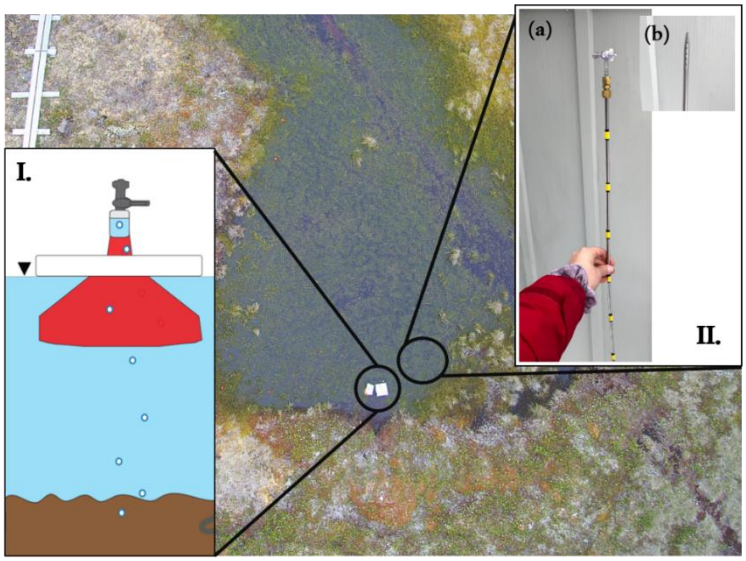

Figure 2. Aerial image of a thaw pond located at Stordalen Mire. (I) CH_4 ebullition samples are collected using a bubble trap floating on the water surface. (II) Dissolved gas porewater samples are collected adjacent to bubble traps to avoid artificial ebullition. A sipper (a) with a perforated end (b) is inserted to depths of 0, 10, 20, and 40cm below the pond bottom to collect 30-ml of water.

hand (McAuliffe, C., 1971). Equilibrated gas samples were then immediately stored in 30-ml evacuated glass vials with butyl rubber septa. Physical limitations such as low daily ebullitive flux and substrates with minimal pore space resulted in uneven sample sizes between individual ponds (Table 1).

Porewater to be analyzed for $\delta^{13}C\text{-}CO_2$ was collected simultaneously with dissolved gas samples in 2014 and 2019 from eight of the nine ponds at depths of 0, 10, 20, and 40cm below the pond bottom. 60-ml polypropylene syringes were used to collect and store 25-ml of porewater that was transported to the ANS to be processed. Samples were stored in 30-ml evacuated glass vials acidified with 0.5-ml of 21% H_3PO_4 and sealed with a butyl rubber stopper.

The headspace of the stored porewater samples collected in 2014 and 2019 was analyzed for concentration and isotopic composition of CH_4 and CO_2 using a continuous-flow Hewlett-

Table 1. Nine thaw ponds at Stordalen Mire were sampled during the growing season over a period of seven years from 2012-2019. Not all ponds were sampled in all years or for both sample types due to field season logistics. Pond type classifications are based on daily ebullitive flux as described in Burke et al. (2019). Sample count is on parentheses next to sample type collected (*n*=).

Pond	Type	Sample type collected	Years sampled
A	1	bubble (*n = 11*) porewater (*n = 56*)	2014, 2016, 2017, 2018, 2019
B	1	bubble (*n = 7*) porewater (*n = 38*)	2014, 2017, 2018, 2019
C	2	bubble (*n = 26*) porewater (*n = 45*)	2012, 2014, 2016, 2017, 2018, 2019
D	2	bubble (*n = 13*) porewater (*n = 31*)	2014, 2016, 2017, 2018, 2019
E	3	bubble (*n = 29*) porewater (*n = 72*)	2014, 2016, 2017, 2018, 2019
F	3	bubble (*n = 43*) porewater (*n = 49*)	2014, 2016, 2017, 2018, 2019
G	4	bubble (*n = 13*)	2012
H	4	bubble (*n = 35*) porewater (*n = 8*)	2012, 2016, 2017, 2018, 2019
X	4	porewater (*n = 11*)	2014

Packard 5890 gas chromatograph (Agilent Technologies) at 40°C coupled to a Finnigan MAT Delta isotope ratio mass spectrometer (GC-IRMS) via a Conflo IV interface system (Thermo Scientific) at Florida State University (FSU) as described by McCalley et al. (2014). This instrument was also used for all ebullition and porewater samples from 2012-2016. In summary, the headspace concentrations were converted to porewater concentrations based on their known extraction efficiencies, defined as the proportion of formerly dissolved gas in the headspace. The extraction efficiency for CO_2 relative to dissolved organic carbon (DIC) was based on the CO_2 extraction from dissolved bicarbonate standards (J. Chanton, personal communication).

II. 4. METHANE ISOTOPE SYSTEMATICS

Isotopic compositions of CH_4 and CO_2 were quantified using the standard delta (δ) notation. This reflects the ratio (*R*) of ^{13}C to ^{12}C or D to H in the sample as a relative difference (denoted as $\delta^{13}C$-CH_4 and δD-CH_4) from the Vienna Pee Dee Belemnite (VPDB) and Standard Mean Ocean Water (SMOW) international standard materials respectively, expressed in per mil (‰) values. An example for C is as follows:

$$\text{Eq 1.}\quad \delta^{13}C = \frac{R - R_{VPDB}}{R_{VPDB}} = \frac{R}{R_{VPDB}} - 1$$

The apparent fractionation factor $CO_2 \rightarrow CH_4$ (α_C) was calculated as:

$$\text{Eq 2.}\quad \alpha_C = \frac{\delta^{13}C\text{-}CO_2 + 1000}{\delta^{13}C\text{-}CH_4 + 1000}$$

Apparent fractionation factor can be interpreted to represent differences in the relative importance of CH_4 production mechanisms with higher α_C indicative of HM and lower α_C indicative of AM (Hornibrook et al., 1997; Michael J. Whiticar, 1999; M.J Whiticar et al., 1986). Fractionation factors can be difficult to estimate in field studies because while CO_2 is the

precursor for CH_4 produced via the hydrogenotrophic pathway, it is not the immediate precursor for the acetoclastic pathway. However, porewater CO_2 is primarily from respiration of organic matter and is isotopically indistinguishable from organic matter enabling a representative fractionation factor to be determined for AM as well (Conrad, 2005; Corbett et al., 2013; Whiticar, 1999). Therefore, dominant CH_4 production mechanisms can be determined by the apparent fractionation factor of a sample.

II. 5. TUNABLE INFRADER LASER DIRECT ABSORPTION SPECTROMETER (TILDAS) MEASUREMENT AND CALIBRATION

Isotopic compositions of CH_4 were measured using a tunable infrared laser direct absorption spectrometer (TILDAS; Aerodyne Research Inc.) located at the Trace Gas Biogeochemistry Laboratory at the University of New Hampshire (UNH) via direct injections. The TILDAS is a modification of the quantum cascade laser spectrometer instruments described by McCalley et al. (2014) and Santoni et al. (2012) and instead allows for manual injection of the sample into the instrument. The TILDAS uses a room-temperature continuous-wave mid-infrared laser whose frequency was tuned to scan rapidly at 900 kHz across $^{12}CH_4$ and $^{13}CH_4$ absorption lines in the 7.5-μm region. The laser light enters a multipass sample cell (effective path length about 200m) containing sample air at low pressure (~5kPa) and is detected by a thermoelectrically cooled detector. The associated TDL-Wintel (Aerodyne Research, Inc.) sampling system software was also used for the analysis. The TDL Wintel program averages high-frequency spectra to produce independent $^{12}CH_4$ and $^{13}CH_4$ mixing ratios in the sample airstream at 1 second intervals, allowing the ratio of ^{13}C-CH_4 to ^{12}C-CH_4 or D-CH_4 to H-CH_4 to be denoted in standard δ notation per mil (‰) as described previously (Equation 1). To keep a reasonable concentration regime for infrared spectroscopic analysis a target mixing ratio of 8ppm

was used. Therefore, all samples are measured at 8ppm with dilution, or at the original concentration if it is already <8ppm. Samples with CH_4 mixing ratios greater than 8ppm are appropriately diluted with zero air via the sampling program. In some cases, the high concentration of ebullition samples required then to be diluted by hand prior to dilution by the sampling program. All ebullition samples were diluted at a ratio of 1ml sample:9 ml room air, as the sample concentration was not always known ahead of time, prior to injection for analysis. If the target mixing ratio (8ppm) was not able to be reached, samples were further diluted by hand and re-run.

Table 2. Isometric standards used to with an Aerodyne calibration system to calibrate three standard tanks at UNH.

Isometric tanks, standards	**$\delta^{13}C$ (‰) ±0.2‰**	**δD (‰)**
B-isol	-54.5	-266
H-isol	-23.9	-171
L-isol	-66.5	-156
T-isol	-38.3	-157

Three working standard calibration tanks were used with the TILDAS at UNH with methane mixing ratios of approximately 2, 5, and 10ppm CH_4. These tanks were calibrated for $\delta^{13}C$-CH_4 and δD-CH_4 using an Aerodyne calibration system containing four Isometric methane isotope standards, each with 2500ppm CH_4. These four primary tanks were calibrated to the VPDM scale via flask samples that were also analyzed for $\delta^{13}C$ by GC-IRMS at FSU, allowing comparable measurements to be made between the two methods. The isotopic methane ratios of each standard are given in Table 2. The δD are considered preliminary calibrations. The precision for δD measurement is ~3‰.

The TILDAS and associated sample analysis system also includes an Alicat flow controller (Alicat Scientific) for each of the three standard tanks, an Alicat on an ultra zero air (dilution flow), a computer with an Igor-based program for calibration control and analysis, RS232 communication between the computer and an Alicat control box, and other valves for automated operation. An Igor-based program selects and sends each standard to the instrument at a controlled flow rate along with the dilution flow for a given period. We selected flows to generate CH_4 levels from approximately 12 ppm to <1ppm via a variable flow rate, and thus span the range of CH_4 levels in this study with manual dilutions. A Keeling plot analysis method was used to determine the relationship between the spectroscopic and the standard isotopic ratios. This linear relationship was then applied to the measured spectroscopic isotopic ratios of the UNH calibration tanks. A fourth tank containing 5% methane was also calibrated (Table 3).

Table 3. $\delta^{13}C$ (‰) and δD (‰) of four standard tanks at UNH used with TILDAS sample analysis.

UNH standard tanks	**$\delta^{13}C$ (‰)**	**δD (‰)**
Low cal tank (~2ppm)	-49.25	5.82
Mid cal tank (~5ppm)	-45.61	-160.22
High cal tank(~9ppm)	-44.19	-143.93
5% CH_4 tank	-37.67	-149.30

II. 6. STATISTICAL ANALYSES

Univariate statistical analyses were performed using the R Project for Statistical Computing (v. 3.5.3) software and the JMP Pro 15 software. Significance of all statistical analyses were determined at the $\alpha = 0.05$ level. Isotopic signature for $\delta^{13}C$-CH_4 and $\delta^{13}D$-CH_4

data was checked for normality using the Anderson-Darling test for normality. Differences in isotopic composition between ponds, pond types, and sample types were assessed using one-way analysis of variance (ANOVA) and the Tukey-Kramer honestly significant different (HSD) test for normally distributed data. Differences in isotopic composition between sampling months and years were assessed using one-way ANOVA and the Tukey-Kramer HSD test for normally distributed data and the Kruskal-Wallis rank sum test and the Dunn's test were used for nonnormal data. A linear regression analysis was used to compare instrumentation methodologies for determining $\delta^{13}C$.

III. RESULTS

III. 1. ISOTOPIC COMPOSITION OF STABLE ISOTOPES OF CH_4 AND CO_2

Our multi-year dataset of stable isotopes of CH_4 ebullition and porewater from eight sub-arctic thaw ponds shows variation in isotopic signature among individual ponds and over time on both monthly and interannual timescales. Overall, the $\delta^{13}C$-CH_4 of ebullition and porewater during the growing season from 2012-2019 ranged from -86.3‰ to -49.2‰ and 98.2‰ to -42.9‰, respectively (Figure 3a, 3b). Porewater $\delta^{13}C$-CH_4 data was normally distributed while ebullition data was not (Table 4). The mean and standard deviation of ebullition $\delta^{13}C$-CH_4 was -66.7 ± 8.6‰ (n=177) and -74.9 ± 8.8‰ (n=313) for porewater $\delta^{13}C$-CH_4 (Table 5). When compared between individual ponds using a one-way ANOVA, mean $\delta^{13}C$-CH_4 of ebullition fell into three significantly different groups (Figure 3b). Pond G ebullition, a Type 4 pond that is fully thawed with high relative amounts of sedge vegetation, was the most enriched and was significantly different from all other ponds. Ponds H and F were more depleted than G and were not significantly different from each other. Ponds C and E were the most depleted and were not significantly different from one another or from ponds A and B. Pond D was not significantly

different from ponds A, B, H, or F (Tukey HSD, $P < 0.001$; Figure 3b). Mean δ^{13}C-CH_4 of porewater was also compared using a one-way ANOVA that resulted in three significantly different groups (Figure 3a). However, the ponds did not fall into the same groupings as were

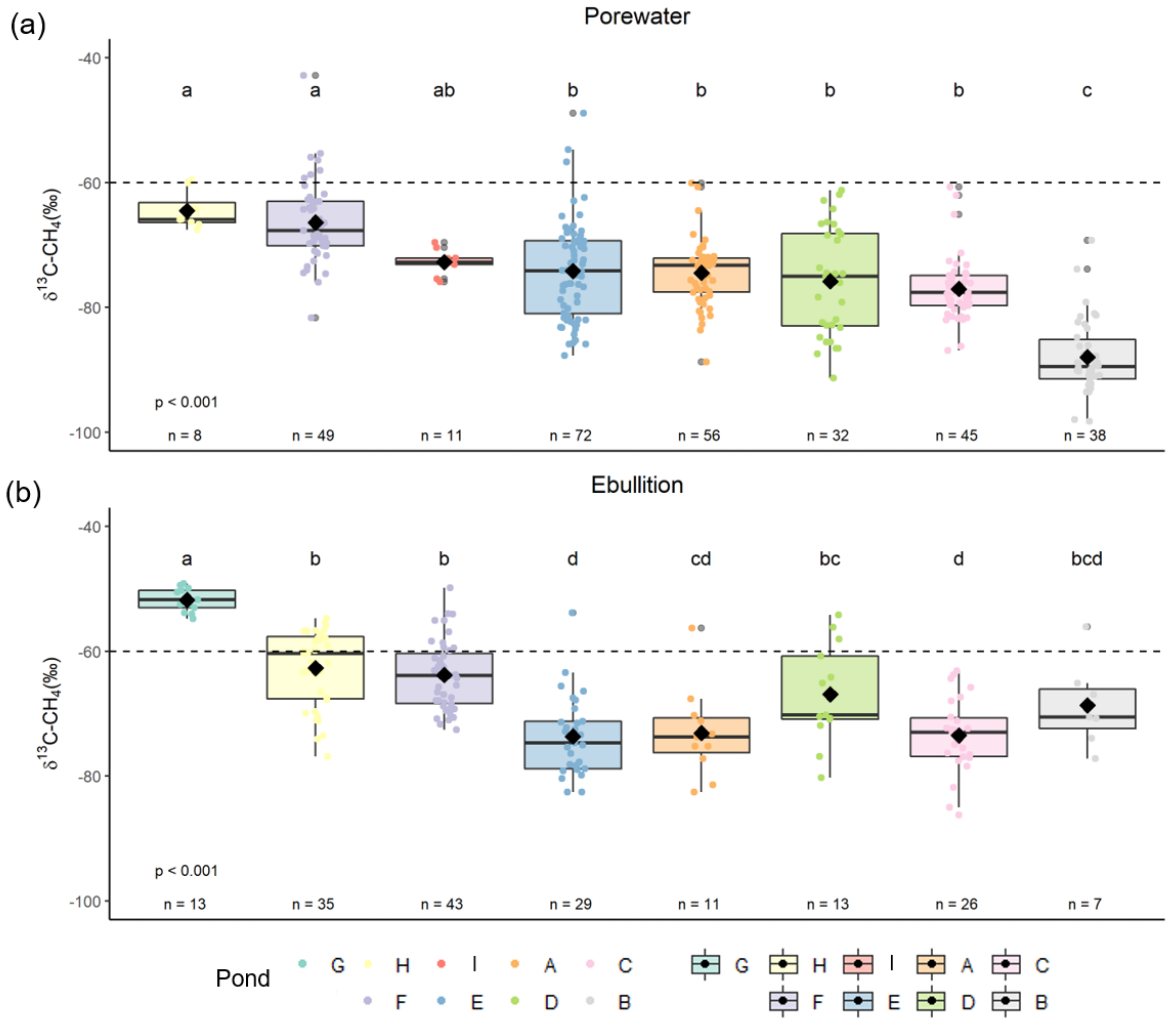

Figure 3. Porewater (a) and ebullition (b) δ^{13}C-CH_4 from 2012-2019 growing seasons grouped by pond. Whiskers represent the 10th and 90th percentiles, and colors indicate different ponds. Black diamonds and horizontal black lines denote means and medians respectively. Lowercase letters along the top of each plot correspond to statistically significant groupings based on a Tukey HSD post-hoc test ($P < 0.001$). Colored points represent individual data points. The number of samples (n) in each group is noted along the bottom. A horizontal dotted black line at -60‰ indicates a transition from greater relative contribution of acetoclastic (-40 to -60‰) to hydrogenotrophic (-60 to -110‰) methanogenesis (Whiticar, 1999). Ponds A and B are Type 1, ponds C and D and Type 2, E and F are Type 3, G, H, and I are Type 4.

seen in ebullition data. Ponds F and H, Type 3 and 4 ponds respectively that are fully thawed with high relative amounts of sedge vegetation, were not significantly different from each other

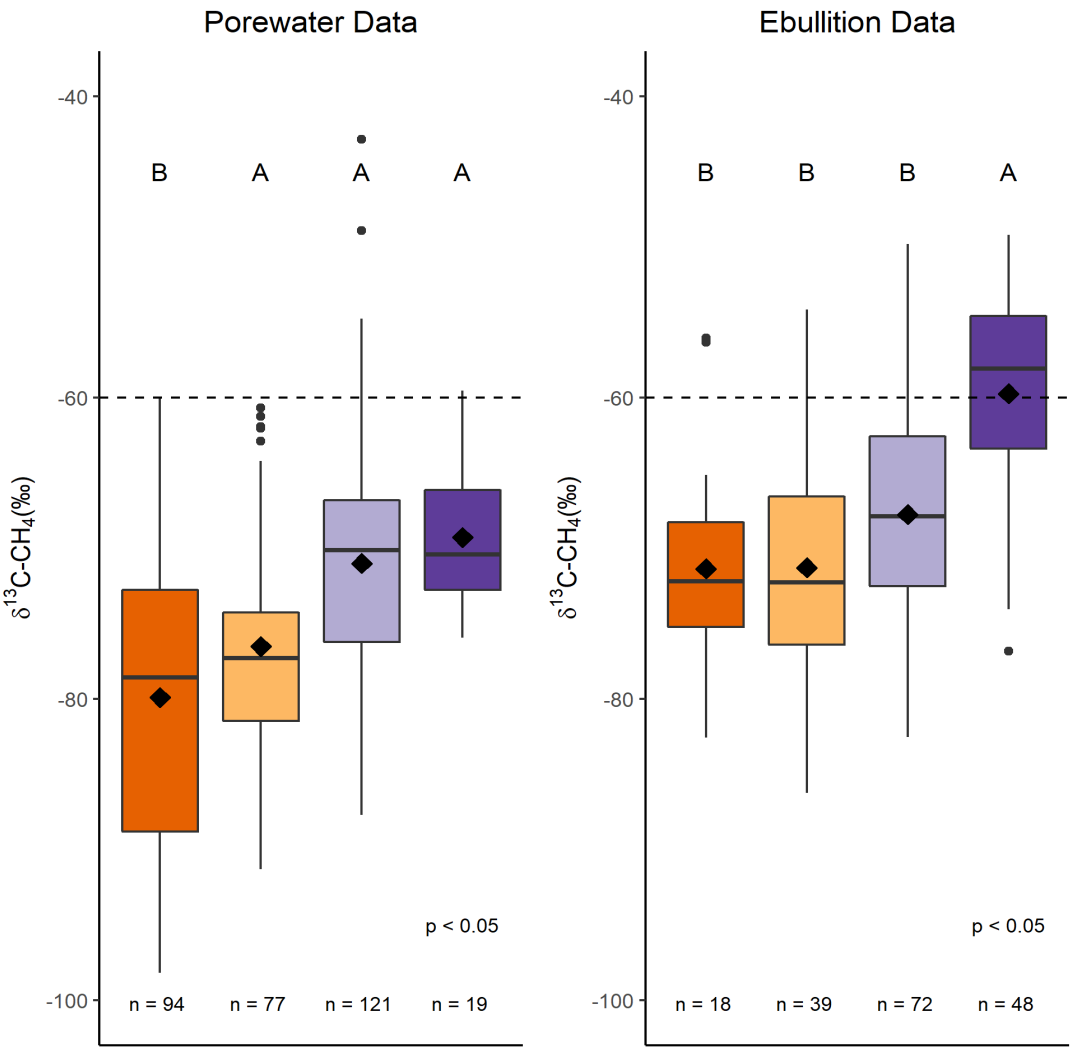

Figure 4. Box plots of porewater (left) and ebullition (right) $\delta^{13}C\text{-}CH_4$ from 2012-2019 sampling years grouped by pond Type. Whiskers represent the 10^{th} and 90^{th} percentiles and black dots represent outliers. Colors indicate different pond Types. Black diamonds and horizontal black lines denote means and medians respectively. Uppercase letters along the top correspond to statistically significant groupings based on a Tukey HSD post-hoc test ($p < 0.05$). The number of samples (n) in each group is noted along the bottom. A horizontal dotted black line at -60‰ indicates a transition from greater relative contribution of acetoclastic (-40 to -60‰) to hydrogenotrophic (-60 to -110‰) methanogenesis (Whiticar, 1999).

and were the most enriched. Ponds E, A, D, and C were not significantly different from each other and were more depleted in $\delta^{13}C\text{-}CH_4$. Pond I was not significantly different from ponds H, F, E, A, D, or C. Pond B was significantly different from all other ponds and had the most depleted mean $\delta^{13}C\text{-}CH_4$ of porewater (Tukey HSD, $P < 0.001$; Figure 2). When grouped by pond Type, $\delta^{13}C\text{-}CH_4$ of porewater and ebullition decrease and become more enriched from pond Type 1 to pond Type 4 (Figure 4). However, pond Type 4 had the only significantly different mean $\delta^{13}C\text{-}CH_4$ of ebullition data and pond Type 1 had the only significantly different mean $\delta^{13}C\text{-}CH_4$ of porewater (Figure 4; $P < 0.05$). In general, $\delta^{13}C\text{-}CH_4$ of ebullition was more enriched than $\delta^{13}C\text{-}CH_4$ of porewater (Table 4). However, mean $\delta^{13}C\text{-}CH_4$ of ebullition and porewater from the same pond with all years combined was not significantly different, except for pond B (Tukey HSD, $P < 0.001$, Figure 3). This was also true when grouped by pond Type, except for pond Type 4 (Tukey HSD, $P < 0.001$, Figure 4).

We examined temporal trends of $\delta^{13}C\text{-}CH_4$ between ponds and found that on a monthly timescale porewater $\delta^{13}C\text{-}CH_4$ is significantly more depleted in September than in June (Figure 5a) while ebullition follows an opposing trend with $\delta^{13}C\text{-}CH_4$ significantly more enriched late in the summer in August than in June (Figure 5b). Pairwise comparisons using the Dunn's test revealed that Pond F was the only pond with significant difference in $\delta^{13}C\text{-}CH_4$ between months for both ebullition and porewater (Table 7, 9, S2, S4). Interannually, porewater $\delta^{13}C\text{-}CH_4$ is relatively stable as five out of six sampling years are not significantly different (Figure 5c). The 2016 sampling season is significantly more enriched than other sampling years, except for 2012 (Figure 5c). Ebullition $\delta^{13}C\text{-}CH_4$ becomes more depleted from 2012 to 2019. Ebullition $\delta^{13}C\text{-}CH_4$ in 2012 is significantly more enriched than data from the 2017 and 2019 sampling seasons but is not significantly different from 2016 and 2018 (Figure 5d). Pairwise comparison using the

Dunn's test determined that Ponds E and H had significant differences in ebullition $\delta^{13}C\text{-}CH_4$ was significantly different between sampling years within ponds E, F and H (Table 6, S1) and ebullition $\delta^{13}C\text{-}CH_4$ was significantly different between sampling months within ponds A, C, D, E, and F (Tables 8, S3). When grouped by pond type, ebullition and porewater $\delta^{13}C\text{-}CH_4$ of Type 3 and 4 ponds were generally more enriched across sampling years while Type 1 and 2 ponds were relatively depleted (Figure 6). Both porewater and ebullition monthly mean $\delta^{13}C\text{-}CH_4$ was generally more enriched for all pond types in 2016, as seen in the porewater data (Figure 5c, 6).

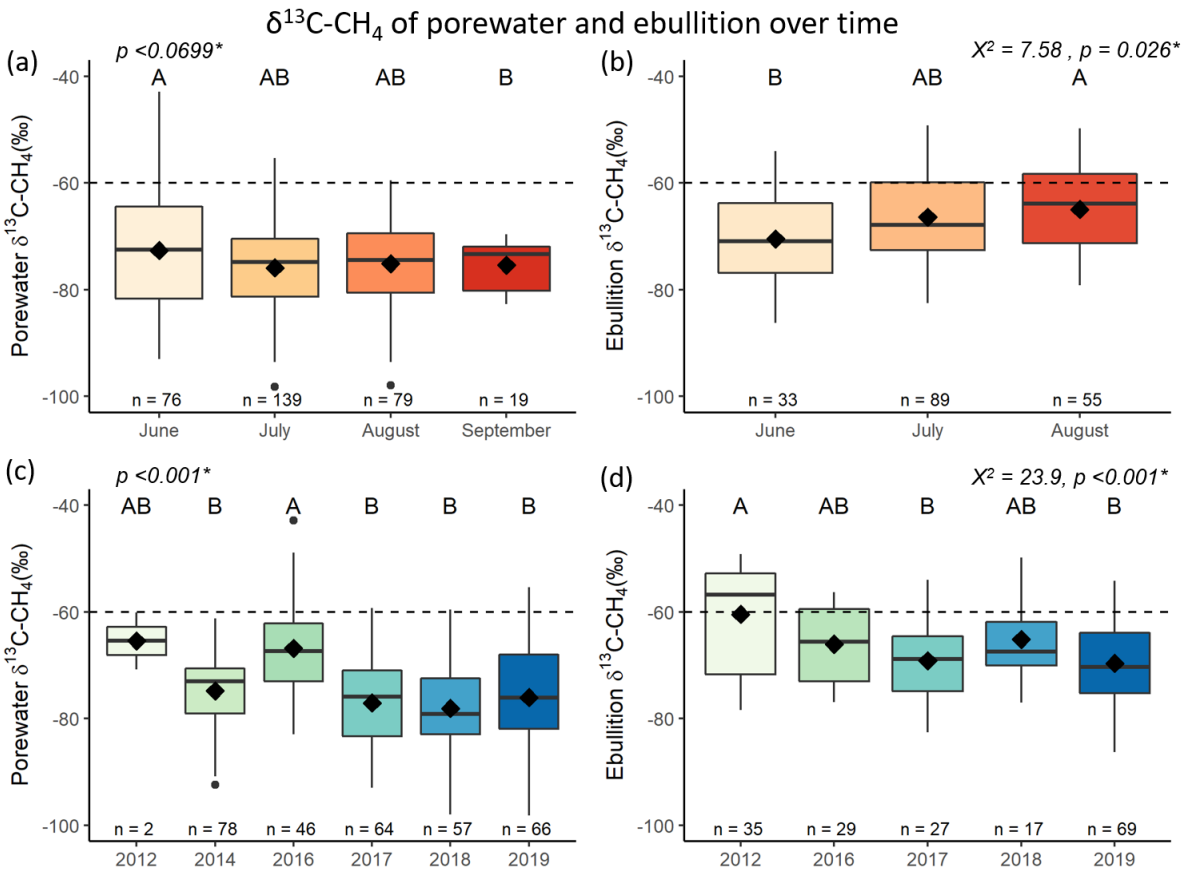

Figure 5. Porewater (a, c) and ebullition (b, d) $\delta^{13}C\text{-}CH_4$ from all ponds grouped by month (a, b) and by year (c, d). Whiskers represent the 10th and 90th percentiles and black dots represent outliers. Black diamonds and horizontal black lines denote means and medians respectively. The number of samples (*n*) in each group is noted along the bottom. A horizontal dotted black line at -60‰ denotes a transition from greater relative contribution of acetoclastic (-40 to -60‰) to hydrogenotrophic (-60 to -110‰) methanogenesis (Whiticar, 1999). 5a and 5c: Mean $\delta^{13}C\text{-}CH_4$ was compared using a one-way ANOVA and a Tukey HSD post-hoc test for data that was normally distributed. Uppercase letters represent significantly different groupings of sampling seasons or months as determined by an all pairs Tukey-Kramer HSD test. Significant p values are marked by *. 5b and 5d: The Kruskal-Wallis rank sum test was used to assess data that did not meet the assumptions for a one-way ANOVA and is plotted as χ^2 and *p*. Uppercase letters indicate pairwise differences between sampling seasons or months as determined by a Dunn's test following the Bonferroni method ($\alpha = 0.05$).

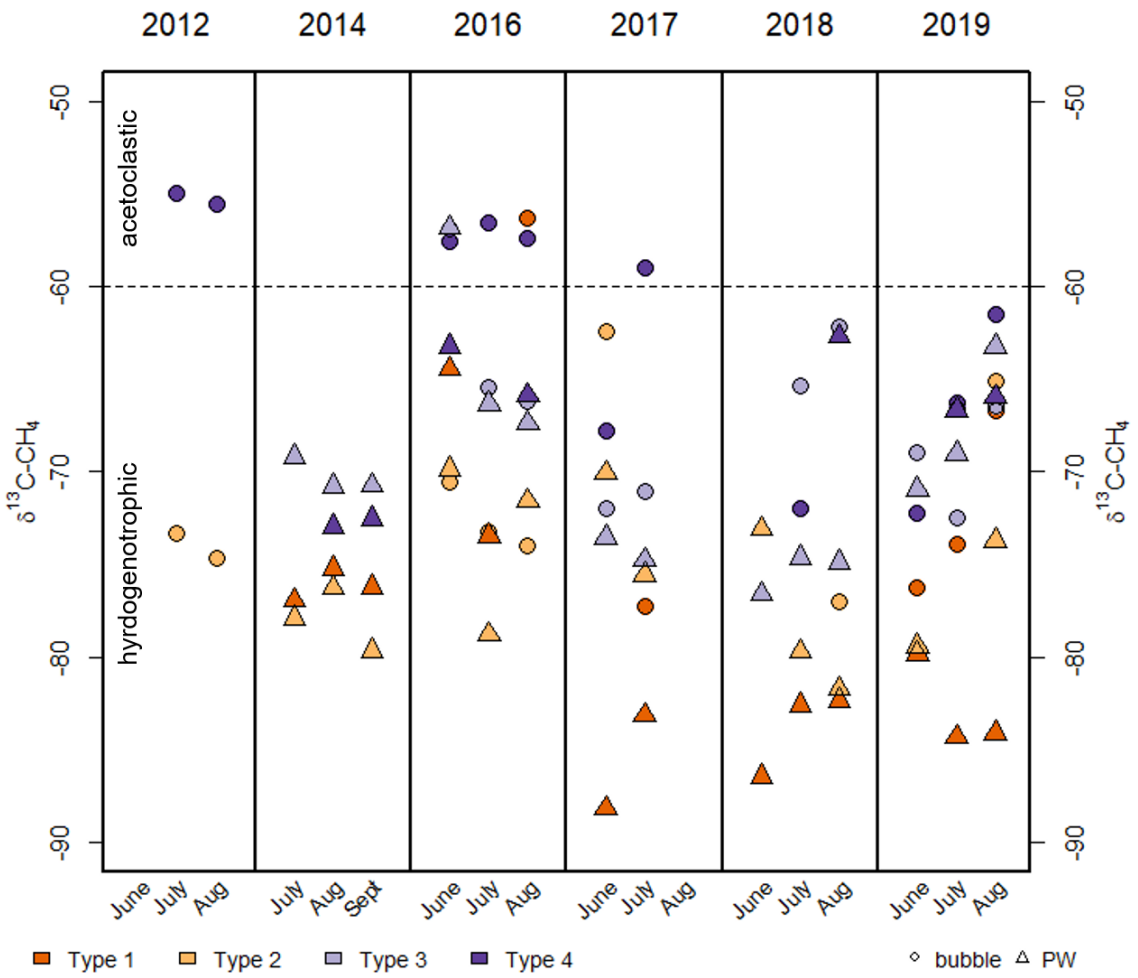

Figure 6. Porewater and ebullition δ^{13}C-CH_4 from 2012-2019 sampling years grouped by pond Type and sample type. Months along the lower x-axis indicate the month of sample collection while years along the upper x-axis indicate year of sample collection. Colors indicate different pond Types while circles and triangles indicate ebullition (bubble) and porewater samples respectively. Points are averages of ≥ 2 data points. A horizontal dotted black line at -60‰ indicates a transition from relative contribution of acetoclastic (-40 to -60‰) to hydrogenotrophic (-60 to -110‰) methanogenesis (Whiticar, 1999). Across and within years δ^{13}C-CH_4 remains relatively constant within pond and sample type.

The δD-CH_4 of bubbles and porewater ranged from -397‰ to -199‰ and from -383‰ to - 184‰, respectively. Ebullition δD-CH_4 data was normally distributed while porewater data was not (Table 4). The mean and standard deviation of bubble δD-CH_4 was -310 ± 44‰ and -315 ± 36‰ for porewater δD-CH_4 (Table 5). Mean δD-CH_4 of ebullition was not statistically different

between individual ponds or when grouped by pond Type (Tukey HSD, P = 0.654 and 0.354). Mean δD-CH_4 of porewater was also not statistically different between individual ponds or when grouped by pond Type (*Tukey HSD*; P =0.867 and 0.958). Mean δD-CH_4 was also not found to be significantly different between ebullition and porewater samples from the same pond or pond Type (Tukey HSD, P = 0.815 and 0.637).

When examining temporal trends in δD-CH_4 we found neither porewater nor ebullition δD-CH_4 was significantly different between sampling months (Figure 7a, 7b). Ebullition δD-CH_4 was also not significantly different between sampling years (Figure 7d), while porewater δD-CH_4 became more depleted from 2017 to 2019 (Figure 7c). 2017 was significantly more enriched that δD-CH_4 porewater data from the 2019 sampling season (Figure 7c).

Table 4. Results of the Anderson-Darling test for normality on δ^{13}C-CH_4 and δD-CH_4 porewater and ebullition data. The hypothesis of normality is rejected for p-values less than or equal to 0.05. Significant p-values indicating a rejection of the hypothesis of normality are noted with *.

Data type	**Sample type**	**A^2**	***p***
δ^{13}C-CH_4	porewater	0.517	0.165
δ^{13}C-CH_4	ebullition	0.914	0.022*
δD-CH_4	porewater	1.669	>0.0001*
δD-CH_4	ebullition	0.341	0.484

We examined isotopic composition of CH_4 (δD-CH_4 and δ^{13}C-CH_4) in years 2017-2019 and found that ebullition data from pond Types 1 and 2 had more enriched mean δD-CH_4 and δ^{13}C-CH_4 than porewater from the same pond types (Figure 8). Ebullition data from Type 3 was more enriched in δ^{13}C-CH_4 compared to porewater from the same pond but did the δD-CH_4 did not differ. Ebullition data from Type 4 had more depleted mean δD-CH_4 and δ^{13}C-CH_4 than

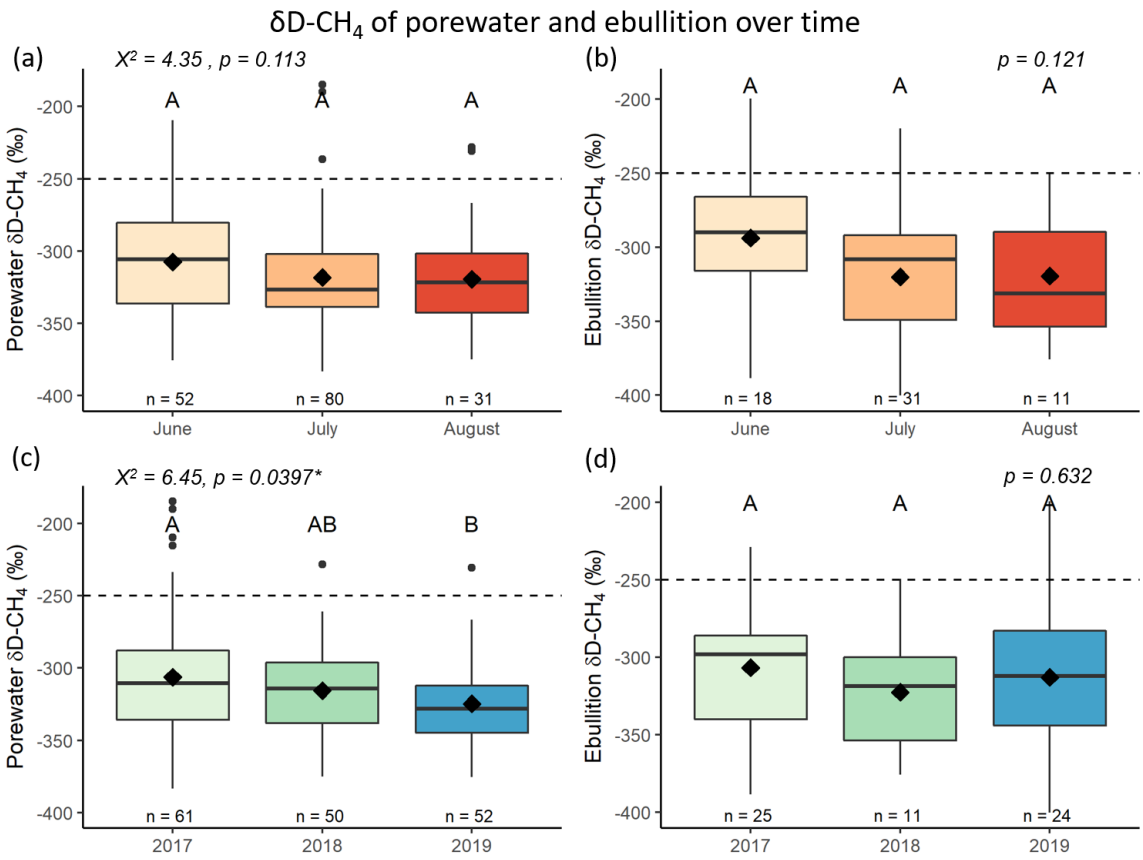

Figure 7. Box plots of porewater (a, c) and ebullition (b, d) δD-CH_4 from all ponds grouped by month (a, b) and by year (c, d). Whiskers represent the 10th and 90th percentiles and black dots represent outliers. Black diamonds and horizontal black lines denote means and medians respectively. The number of samples (*n*) in each group is noted along the bottom. A horizontal dotted black line at -250‰ denotes a transition from greater relative contribution of hydrogenotrophic (-170to -250‰) to acetoclastic (-250 to -400‰) methanogenesis (Whiticar, 1999). Significant p values are marked by *. 7a and 7c: The Kruskal-Wallis rank sum test was used to assess data that did not meet the assumptions for a one-way ANOVA and is plotted as χ^2 and *p*. Uppercase letters indicate pairwise differences between sampling seasons or months as determined by a Dunn's test following the Bonferroni method ($\alpha = 0.05$). 7b and 7d: Mean δ^{13}C-CH_4 was compared using a one-way ANOVA and a Tukey HSD post-hoc test for data that was normally distributed. Uppercase letters represent significantly different groupings of sampling seasons or months as determined by an all pairs Tukey-Kramer HSD test.

porewater from the same pond type. Mean δ^{13}C-CH_4 of porewater became increasingly more enriched moving from Type 1 to Type 4 however, mean δD-CH_4 of porewater varied minimally between pond Types. Mean δD-CH_4 of ebullition was the most enriched in pond Type 2 and the

most depleted in pond type 4. Mean $\delta^{13}C\text{-}CH_4$ of ebullition was most depleted in Type 1 and most enriched in Type 4 (Figure 8). We compared isotopic composition of dissolved CH_4 in porewater by depth from 2017-2019 and found pond type to be more indicative of isotopic composition than depth (Figure 9). Mean $\delta^{13}C\text{-}CH_4$ from all depths of 0 to 40cm was most depleted in Type 1 and most enriched in Type 4. Mean $\delta D\text{-}CH_4$ fell within a narrow range of -336 to -298‰ across depths and pond types (Figure 9).

In addition to $\delta^{13}C\text{-}CH_4$, the $\delta^{13}C\text{-}CO_2$ of pond porewater was measured in 2014 and 2019. Porewater $\delta^{13}C\text{-}CO_2$ when years were grouped together ranged from -22.2 to 5.6‰ with a mean and standard deviation of -10.4 ± 6.5‰ *(n = 166*) and differed significantly between pond Types (Table 5, Figure 10a). Pond Type 3 was the most enriched and varied significantly from pond Types 1, 2 which were more depleted. Pond Type 4 was not significantly different from any other pond Type (Tukey HSD, $P < 0.001$; Table 5; Figure 10a).

Table 5. Mean ebullition and porewater $\delta^{13}C\text{-}CH_4$, $\delta D\text{-}CH_4$, $\delta^{13}C$-DIC, and fractionation factor (α) from four pond Type classifications. Mean $\delta^{13}C\text{-}CH_4$ contains data from all sampling years. Mean $\delta D\text{-}CH_4$ contains data from 2017-2019 sampling seasons. Mean $\delta^{13}C$-DIC and α are from porewater samples collected during the 2014 and 2019 sampling seasons. from 2014 and 2019.

Pond Type	Ebullition $\delta^{13}C\text{-}CH_4$ (‰)	Porewater $\delta^{13}C\text{-}CH_4$ (‰)	Ebullition $\delta D\text{-}CH_4$ (‰)	Porewater $\delta D\text{-}CH_4$ (‰)	Porewater $\delta^{13}C\text{-}CO_2$ (‰)	Porewater α_C
1	-71.37 ± 7.18	-79.92 ± 8.58	-294 ± 41	-283 ± 27	-10.67 ± 7.16	1.073 ± 0.0057
2	-71.29 ± 7.29	-76.52 ± 6.79	-315 ± 40	-317 ± 66	-13.34 ± 5.22	1.069 ± 0.0060
3	-67.78 ± 7.60	-71.01 ± 8.16	-315 ± 34	-317 ± 39	-7.11 ± 5.28	1.066 ± 0.0084
4	-59.74 ± 7.25	-69.28 ± 4.78	-313 ± 35	-309 ± 54	-9.33 ± 5.11	1.067 ± 0.0072

The apparent fractionation factor (α_C) calculated from porewater $\delta^{13}C\text{-}CO_2$ and $\delta^{13}C\text{-}CH_4$ ranged from 1.046 to 1.083 with a mean and standard deviation of 1.07 ± 0.01 (*n = 162*; Table 5,

Figure 10b). Mean α_C of porewater varied significantly between pond Type with years grouped together when compared using a one-way ANOVA. Pond Type 1 had the highest mean α and was significantly different from pond Types 3 and 4. Pond Types 3 and 4 had lower mean α and were not significantly different from each other. Pond Type 2 was not significantly different from pond Types 1, 3, or 4 (Figure 10b; Table 1; $P < 0.001$). Mean α did not differ between sampling years of 2014 and 2019, except for pond Type 4 which had a lower mean α in 2019 than in 2014 (Figure 11). Pond Type 1 porewater in 2019 had the most depleted mean $\delta^{13}C\text{-}CH_4$ while pond Type 4 was the most enriched. Porewater from pond Type 1 in 2019 has the highest mean α value while pond Type 4 in 2019 has the lowest. Mean α of pond Types 3 and 4 both decrease between 2014 and 2019 while pond Type 2 does not (Figure 11).

III. 2. METHOD COMPARISON

Porewater $\delta^{13}C\text{-}CH_4$ samples were analyzed using either a QCLS or a GC-IRMS. A linear regression analysis determined a positive correlation between $\delta^{13}C\text{-}CH_4$ from the two sample methods. The linear model y = 0.84x – 13.9 fit 80% of the samples ($P < 2.2e\text{-}16$, $R^2 = 0.80$; Figure 12). The QCL and GC-IRMS methods yielded similar results for data from the 2019 growing season, allowing data from sampling years and methods to be combined to make interannual and conclusions.

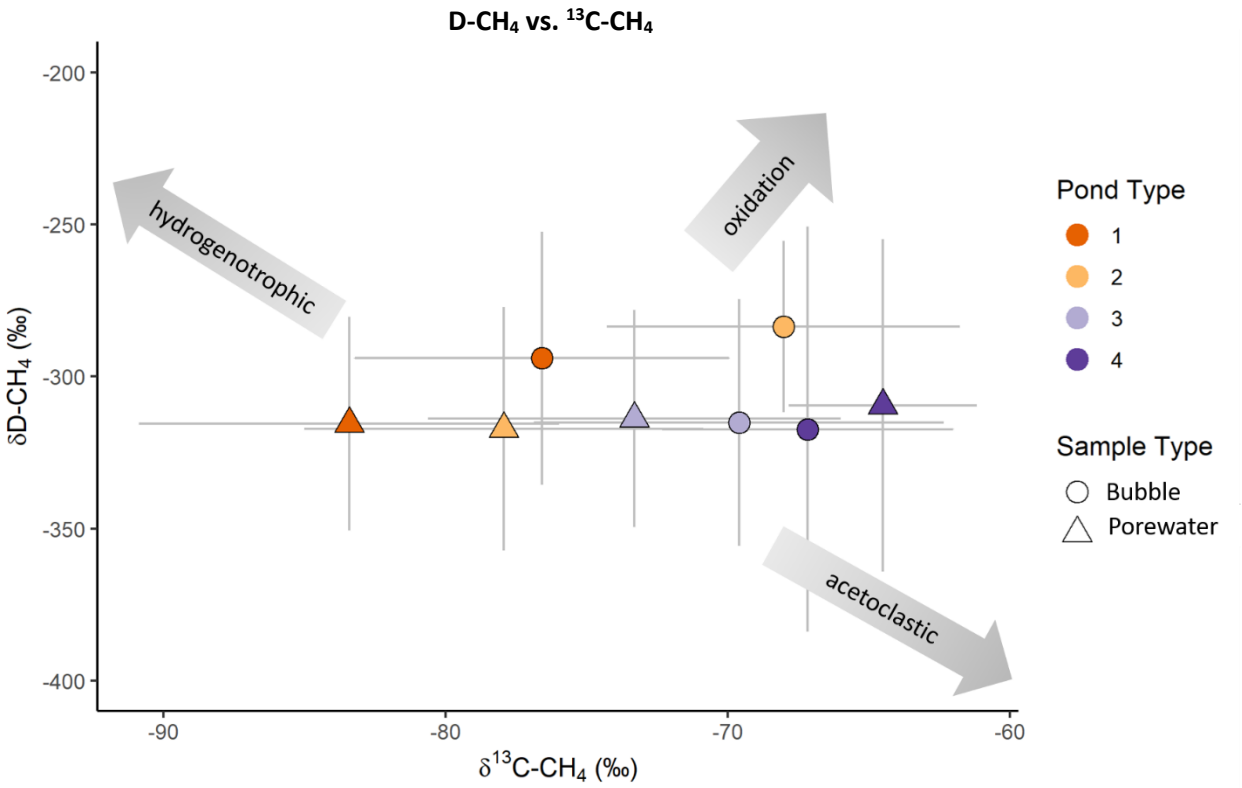

Figure 8. Average porewater and ebullition δD-CH_4 and δ^{13}C-CH_4 from 2017-2019 sampling years grouped by pond type and sample type. Different pond types are indicated in distinctive colors, and circles and triangles represent ebullition (bubble) and porewater samples respectively. Light gray lines denote standard deviation around the average values found for each pond type. Gray arrows indicate greater contributions of the denoted methanogenesis pathways or oxidation (Chanton et al., 2005).

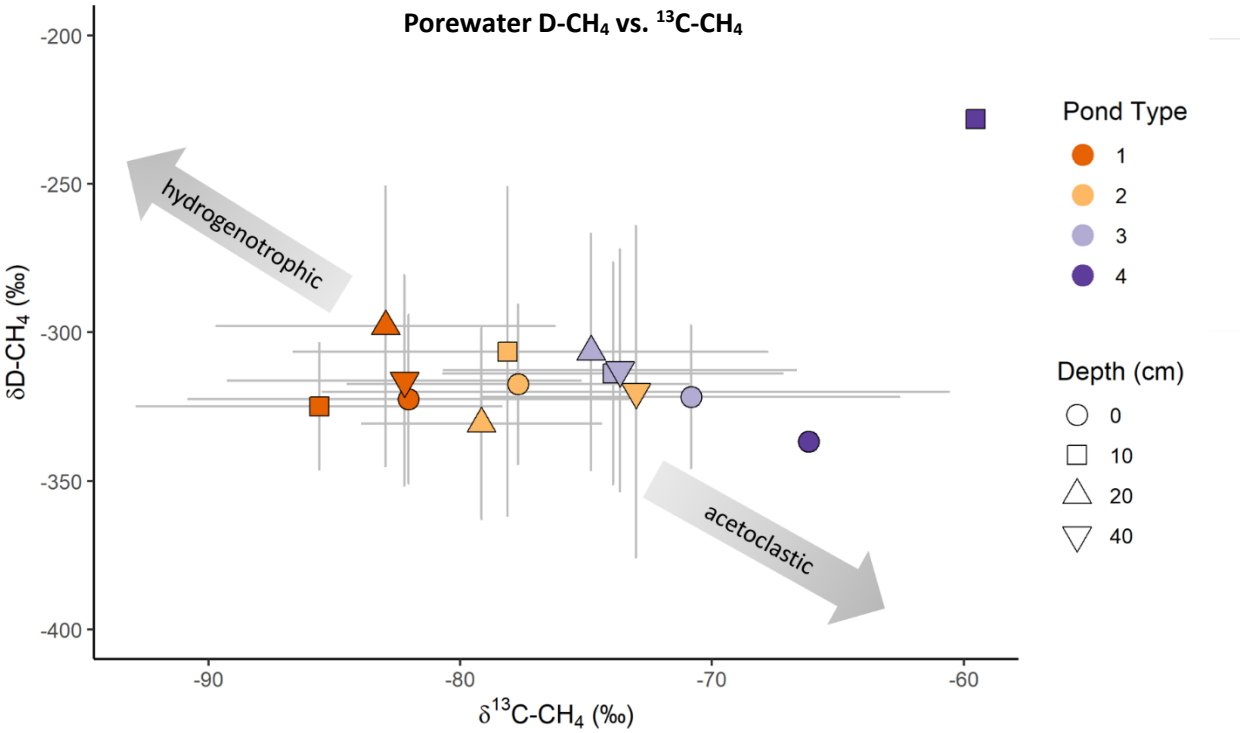

Figure 9. Average porewater δD-CH_4 and δ^{13}C-CH_4 from 2017-2019 sampling years grouped by pond type and depth. Different pond types are indicated in distinctive colors, and shapes denote different sampling depths. Standard deviation is depicted with light gray around the average values found in the pond type. Pond type is a stronger indicate of isotopic composition of δ^{13}C -CH_4 than depth as pond types fall into distinct groups but depth increments do not. Gray arrows indicate greater contributions of the denoted methanogenesis pathways (Chanton et al., (2005).

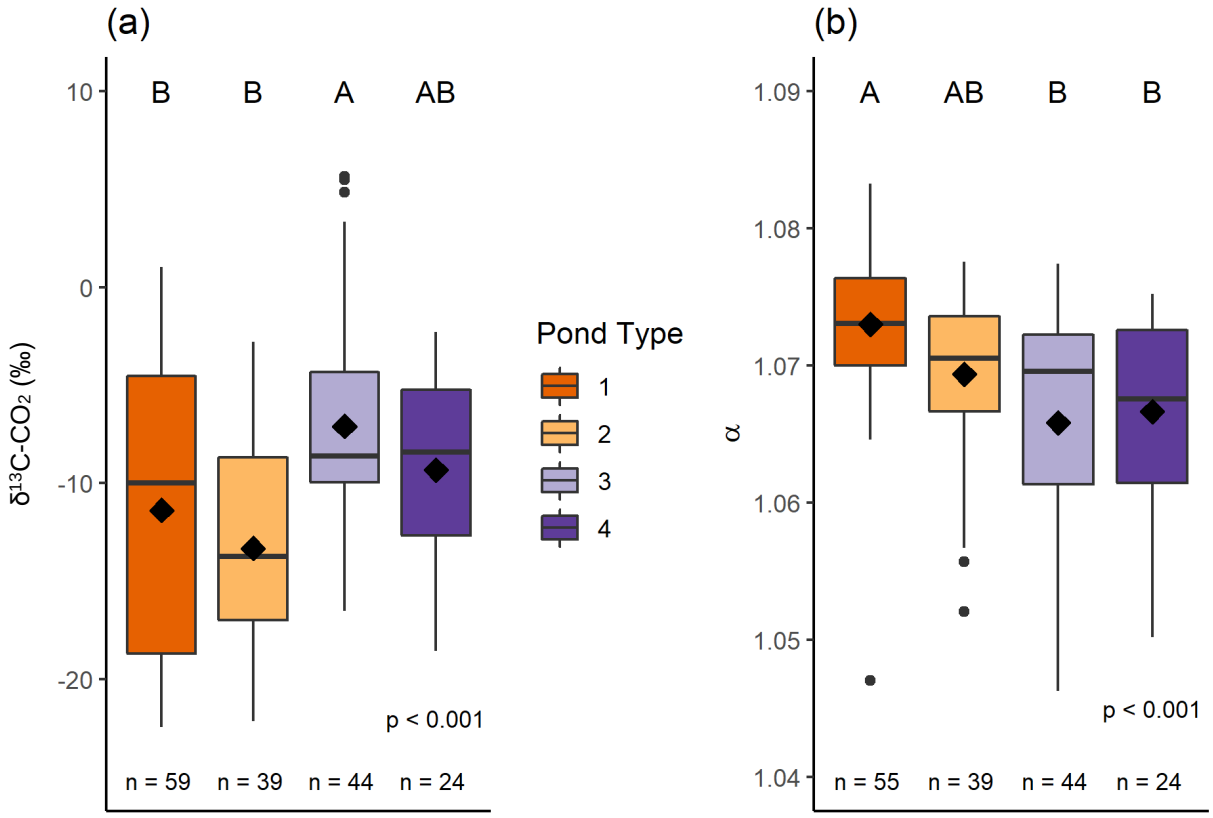

Figure 10. Porewater (a) $\delta^{13}C\text{-}CO_2$ and (b) fractionation factor (α) from 2014 and 2019 sampling years grouped by pond type. Whiskers represent the 10^{th} and 90^{th} percentiles and black dots represent outliers. Colors indicate different pond types. Black diamonds and horizontal black lines denote means and medians respectively. Uppercase letters along the top correspond to statistically significant groupings based on a Tukey HSD post-hoc test ($p < 0.001$). The number of samples (n) in each group is noted along the bottom.

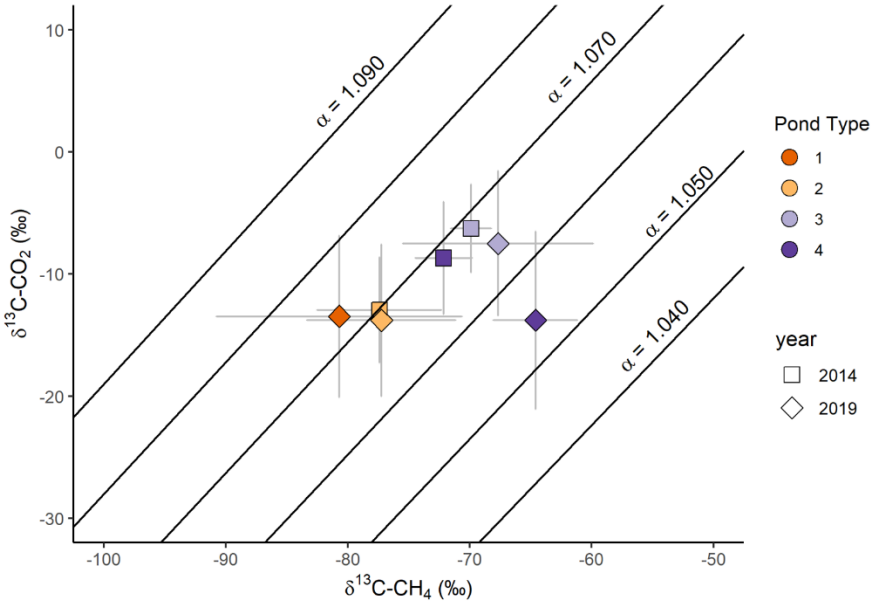

Figure 11. Average porewater δC-CO_2 and δ^{13}C-CH_4 from 2014 and 2019 sampling years grouped by pond type. Standard deviation is depicted with light gray around the average values found for each pond type. Pond types are indicated in distinctive colors, and shapes denote different sampling years. Black lines mark slope of differing fractionation factor (α_c) at 0.01 intervals.

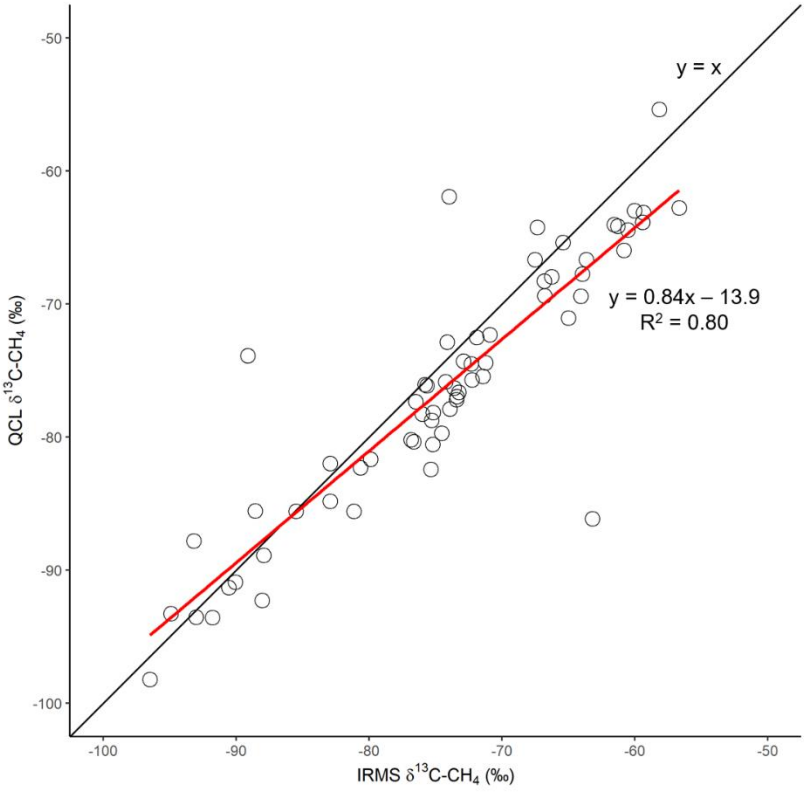

Figure 12. Porewater δ^{13}C-CH_4 from the 2019 sampling season analyzed using both a QCLS and a GC-IRMS. Circles represent individual data points. A black diagonal line represents the 1:1 line. The linear regression model with had an equation of y = 0.84x – 13.9, *P-value* < 2.2*e*-16, and an R^2 value of 0.80 determining that 80% of the data fit the linear regression model, determining that data analyzed with the two methods is comparable.

Table 6. Comparison of ebullition $\delta^{13}C\text{-}CH_4$ by year for each pond using the Kruskal-Wallis rank sum test. *P* values less than or equal to 0.05 indicate significant differences between sampling years within a pond and are marked with a *. See table S1 for corresponding pairwise comparisons.

Ebullition $\delta^{13}C\text{-}CH_4$ by year

Site	χ^2	DF	*p*
Pond A	3.1313	2	0.209
Pond B	NA	NA	NA
Pond C	4.5691	4	0.334
Pond D	3.5027	2	0.173
Pond E	9.6903	3	0.0214*
Pond F	9.0192	3	0.0290*
Pond G	NA	NA	NA
Pond H	17.9995	4	0.0012*
Pond I	NA	NA	NA

Table 7. Comparison of ebullition $\delta^{13}C\text{-}CH_4$ by month for each pond using the Kruskal-Wallis rank sum test. Comparison with 1 degree of freedom (DF) were conducted using the Wilcoxon rank sum test. *P* values less than or equal to 0.05 indicate significant differences between sampling months within a pond and are marked with a *. See table S2 for corresponding pairwise comparisons.

Ebullition $\delta^{13}C\text{-}CH_4$ by month

Site	χ^2	DF	*p*
Pond A	3.4545	2	0.1778
Pond B	3.1429	2	0.2077
Pond C	0.0043	2	0.9979
Pond D	3.0945	2	0.2128
Pond E	5.3891	2	0.0676
Pond F	6.0929	2	0.0475*
Pond G	0.7143	1	0.398
Pond H	5.0238	2	0.0811
Pond I	*NA*	*NA*	*NA*

Table 8. Comparison of porewater $\delta^{13}C\text{-}CH_4$ by year for each pond using a one-way ANOVA. *P* values less than or equal to 0.05 indicate significant differences between sampling years within a pond and are marked with a *. See table S3 for corresponding pairwise comparisons.

Porewater $\delta^{13}C\text{-}CH_4$ by year

Site	DF	*p*
Pond A	4	<0.0001*
Pond B	3	0.3554
Pond C	4	0.0294*
Pond D	4	0.0199*
Pond E	4	<0.0001*
Pond F	4	<0.0001*
Pond G	*NA*	*NA*
Pond H	2	0.571
Pond I	*NA*	*NA*

Table 9. Comparison of porewater $\delta^{13}C\text{-}CH_4$ by month for each pond using a one-way ANOVA. When degrees of freed (DF) was equal to one a pooled t-test was used. *P* values less than or equal to 0.05 indicate significant differences between sampling months within a pond and are marked with a *. See table S4 for corresponding pairwise comparisons.

Porewater $\delta^{13}C\text{-}CH_4$ by month

Site	DF	*p*
Pond A	3	0.0916
Pond B	3	0.183
Pond C	3	0.0899
Pond D	3	0.382
Pond E	3	0.2778
Pond F	3	0.0256*
Pond G	*NA*	*NA*
Pond H	2	0.7216
Pond I	1	0.7241

Table 10. Comparison of porewater δD-CH_4 by month for each pond using the Kruskal-Wallis rank sum test. Comparison with 1 degree of freedom (DF) were conducted using the Wilcoxon rank sum test. *P* values less than or equal to 0.05 indicate significant differences between sampling months within a pond and are marked with a *.

Porewater δD-CH_4 by month

Site	χ^2	DF	*p*
Pond A	0.9001	2	0.6376
Pond B	0.8549	2	0.6522
Pond C	1.4433	2	0.486
Pond D	0.4558	2	0.7962
Pond E	2.9655	2	0.227
Pond F	5.4652	2	0.0651
Pond G	*NA*	*NA*	*NA*
Pond H	0.2	1	0.6547
Pond I	*NA*	*NA*	*NA*

Table 11. Comparison of porewater δD-CH_4 by year for each pond using the Kruskal-Wallis rank sum test. Comparison with 1 degree of freedom (DF) were conducted using the Wilcoxon rank sum test. *P* values less than or equal to 0.05 indicate significant differences between sampling months within a pond and are marked with a *.

Porewater δD-CH_4 by year

Site	χ^2	DF	*p*
Pond A	1.5103	2	0.4699
Pond B	4.5048	2	0.1051
Pond C	1.7888	2	0.4088
Pond D	1.0911	2	0.5795
Pond E	1.2511	2	0.535
Pond F	2.0595	2	0.3571
Pond G	*NA*	*NA*	*NA*
Pond H	2.4	1	0.1213
Pond I	*NA*	*NA*	*NA*

Table 12. Comparison of ebullition δD-CH_4 by month for each pond using a one-way ANOVA. When degrees of freedom (DF) was equal to 1 a pooled t-test was used. *P* values less than or equal to 0.05 indicate significant differences between sampling years within a pond and are marked with a *.

Ebullition δD-CH_4 by month

Site	DF	*p*
Pond A	1	0.8838
Pond B	*NA*	*NA*
Pond C	*NA*	*NA*
Pond D	1	0.8862
Pond E	2	0.2004
Pond F	2	0.3092
Pond G	*NA*	*NA*
Pond H	1	0.1223
Pond I	*NA*	*NA*

Table 13. Comparison of ebullition δD-CH_4 by year for each pond using a one-way ANOVA. When degrees of freedom (DF) was equal to 1 a pooled t-test was used. *P* values less than or equal to 0.05 indicate significant differences between sampling years within a pond and are marked with a *.

Ebullition δD-CH_4 by year

Site	DF	*p*
Pond A	1	0.9606
Pond B	*NA*	*NA*
Pond C	*NA*	*NA*
Pond D	*NA*	*NA*
Pond E	2	0.5046
Pond F	2	0.0486*
Pond G	*NA*	*NA*
Pond H	2	0.5113
Pond I	*NA*	*NA*

IV. DISCUSSION

IV. 1. CONTRIBUTION OF METHANOGENESIS PATHWAYS VARY BY POND TYPE

The isotopic composition of ebullitive and dissolved CH_4 from nine thaw ponds over a seven-year period indicate that relative contribution of methanogenesis pathway differs between ponds and pond types. Ponds A and B, categorized as Type 1, and ponds C and D, categorized as Type 2 have relatively low $\delta^{13}C\text{-}CH_4$ (Table 5, Figure 3, 4)and high α_C (Table 5, Figure 11) suggesting that HM contributes more to production than AM in Type 1 and 2 ponds. Methane produced by relatively higher contribution of HM has been observed to be depleted in the range of -60 to -110‰ for $\delta^{13}C\text{-}CH_4$ and enriched in δD resulting in values ranging from -170 to -250‰ (Chanton et al., 2005; Whiticar, 1999; Whiticar et al., 1986). However, $\delta D\text{-}CH_4$ from Type 1 ebullition (-219±45 to -337±47‰) and porewater (-190±18 to -383±26‰) falls within a range generally observed with higher relative contribution of AM. The same is also true for Type 2 $\delta D\text{-}CH_4$ of ebullition (-249±15 to -324±31‰) and porewater (-184±29 to -365±25‰; Table 5). Methane produced by higher relative contribution of AM, has been observed to enrich in $\delta^{13}C$ and deplete in δD, ranging from -40 to -60‰ and -250 to -400‰, respectively (Chanton et al., 2005; M.J Whiticar et al., 1986). The mean $\delta D\text{-}CH_4$ of pond Type 1 and Type 2 are similar to values found by Jansen et al. (2019) in post-glacial lake sediment gas pockets (-308± 43‰) and to ebullition measurements (-310.6± 21.3‰) from the same lakes by Wik et al. (2020) during the summer months from three lakes located at Stordalen Mire suggesting that these depleted δD values are likely driven by $\delta D\text{-}H_2O$ of source H_2O, which has been documented to heavily influence $\delta D\text{-}CH_4$, rather than by production effects (Chanton et al., 2006; Waldron et al., 1999). HM having higher relative contribution to production in Types 1 and 2 is further supported by

their respective mean α_C (Table 1). Larger α_c values are observed when HM contributes more to production relative to AM while lower α_c indicates higher relative contribution of AM (Chanton et al., 2005; Michael J. Whiticar, 1999; M.J Whiticar et al., 1986). Fractionation factor (α_C) decreases from Type 1 to Type 4 indicating a transition between pond types from higher relative contribution of HM to higher contribution of AM (Figure 10b, Figure 11). Type 1 ponds are hydrologically isolated, the shallowest ponds in this study, and located on palsa plateaus with a low amount of sedge vegetation relative to the other pond types. Type 2 ponds have more sedge vegetation than Type 1 but less than Types 3 and 4, are hydrologically isolated with the exception of Pond D, and are bordered by collapsing palsas (Burke et al., 2019). The presence of hydrogenotrophic methanogenesis in Types 1 and 2 implies the presence of decomposed organic matter and low redox potential (Eh) (Bouchard et al., 2015; Walter et al., 2008). The presence of intact palsas containing decomposed organic matter in the form of peat around Types 1 and 2 supports that these ponds would have a higher relative contribution of hydrogenotrophic methanogenesis than ponds with less access to this form of organic matter. Hydrogenotrophic methanogenesis contributes more to production in pond Types 1 and 2 but will have a low influence on ecosystem scale isofluxes as Types 1 and 2 have a relatively low associated daily ebullitive fluxes (Burke et al., 2019)

While still within ranges observed with higher relative contribution of HM, Types 1 and 2 have ebullition signatures that are enriched in both $\delta^{13}C\text{-}CH_4$ and $\delta D\text{-}CH_4$ in comparison to the associated porewater. This is likely a result of CH_4 oxidation driving enrichment of residual CH_4 in both $\delta^{13}C$ and δD (Chanton et al., 2005). Oxidation has been documented to influence isotopic composition of CH_4 from ebullition of nearby post-glacial lakes at Stordalen Mire (Wik et al., 2020). Methane oxidation in the water column can shift $\delta^{13}C\text{-}CH_4$ up to +20‰ between sediment

bubble CH_4 and dissolved CH_4 (Jansen et al., 2019) however, the shallow nature of the ponds in this study (≤85cm) make it unlikely that oxidation is able to happen in the water column and may instead be occurring in the sediment before bubbles are released to the water surface (Burke et al., 2019; Chanton, 2005; Wik et al., 2020).

Pond Type 3, consisting of ponds E and F, appears to be transitional reflecting a relatively even mix of HM and AM contributing to production. The $\delta^{13}C\text{-}CH_4$ values for Type 3 were significantly more depleted in $\delta^{13}C\text{-}CH_4$ than Types 1 and 2 but still within the range of values indicative of higher relative contribution of HM. There is likely a mixture of HM and AM contributing to production in Type 3 driving the enrichment of $\delta^{13}C\text{-}CH_4$ (Chanton et al., 2005; Whiticar et al., 1986).

The respective ranges of $\delta^{13}C\text{-}CH_4$ and $\delta D\text{-}CH_4$ associated with different production pathways have overlap and can vary based on the isotopic composition of parent organic material, kinetic isotope fractionation, and mixture of the two production pathways resulting in a "transitional" isotopic composition between hypothesized ranges (Whiticar, 1999). Additionally, some question remains on the applicability of these ranges to freshwater systems (Wik et al., 2020) being originally based on isotopic data from marine environments (Whiticar et al., 1986). Apparent fractionation factor (α_C) can be useful to reconcile these overlaps and distinguish production pathways as fractionation from production remains somewhat constant despite variances in source $\delta^{13}C$ and δD (Whiticar, 1999). Type 3 has a significantly lower mean α_C (1.046 to 1.077) than Type 1 with sample years combined, further supporting a shift towards higher relative contribution of AM in Type 3 ponds compared to Types 1 and 2 (Figure 10b; Chanton et al., 2005; Whiticar, 1999; Whiticar et al., 1986). Between 2014 and 2019 the mean α_C of Type 3 decreases (Figure 11) reflecting a possible shift over time towards more contribution

of AM that is not seen in $\delta^{13}C\text{-}CH_4$ alone (Figure 6). As the highest emitting pond type (Burke et al., 2019), shifts in the relative contribution of methanogenesis pathway and the associated isotopic composition of Type 3 emissions over time has the greatest potential relative to other pond types to influence isotopic composition at the ecosystem scale.

In Type 4, consisting of ponds G, H, and X, isotopic analysis indicates that AM and HM both contribute to production but AM has a higher relative contribution than is seen in Types 1-3. Mean $\delta^{13}C\text{-}CH_4$ of Type 4 is significantly more enriched in ebullition (-49.2 to -76.8±0.50‰) than in porewater (-59.5±0.51 to -75.9±0.14‰), though this is likely driven by inconsistent sampling between individual ponds and less a reflection of oxidation effects that could explain enriched $\delta^{13}C$ between the sediment and emitted bubbles within a particular pond (Table 1; Chanton et al., 2005). Regardless of significant differences in mean $\delta^{13}C\text{-}CH_4$ of individual ponds and between porewater and ebullition, the overall mean $\delta^{13}C\text{-}CH_4$ of Type 4 ponds was the most enriched of all pond types, significantly so for ebullition data (Table 2; Figure 2). Enriched mean $\delta^{13}C\text{-}CH_4$ of ebullition indicates higher contribution AM relative to other pond Types and mean $\delta^{13}C\text{-}CH_4$ of porewater was also enriched in the transitional range of $\delta^{13}C$ values where contribution of both pathways is common, as seen is Type 3 (Chanton et al., 2005; Whiticar, 1999; Whiticar et al., 1986). Type 4 $\delta D\text{-}CH_4$ of ebullition (-199±42 to -397±127‰) and porewater (-228±17 to -339±27‰) is depleted within ranges hypothesized for higher contribution of AM (Chanton et al., 2006; Whiticar, 1999; Whiticar et al., 1986). The pairing of enriched $\delta^{13}C\text{-}CH_4$ and depleted $\delta^{13}C\text{-}CH_4$ suggest AM has a large relative contribution to production in Type 4 ponds and is further supported by fractionation factor (α_c) (Chanton et al., 2005). The relatively low mean α_c of Type 4 supports a larger role of AM compared to Types 1-3 (Figure 10; Chanton et al., 2005; Whiticar, 1999; Whiticar et al., 1986). The relatively high

contribution of AM coincides with relatively high CH_4 daily ebullitive flux from Type 4 ponds and an increased presence of *Carex spp.* and *Eriophorum spp.* sedge vegetation compared to other pond Types (Burke et al., 2019). Type 4 ponds are hydrologically connected to the surrounding mire complex with input from adjacent fen areas, potentially explaining the shift in relative contribution of production pathway as increased hydrologic conductivity provides an input of labile C substrates favorable for AM (Hornibrook et al., 1997).

IV. 2. THAW PROGRESSION SHIFTS METHANOGENESIS PATHWAY

The four pond types in this study are representative of different thaw stages and their differences in dominant methanogenic pathway suggest a shift from higher relative contribution of HM to more contribution from AM as thaw stage progresses. Type 1 ponds are located on a palsa plateau while Type 2 ponds are located along edges of collapsed palsa, suggesting a chronological order between pond types as permafrost thaw and active layer deepening cause progression from Type 1 to Type 2 (Burke et al., 2019; Olsen et al., 2011). The mean $\delta^{13}C\text{-}CH_4$ of ebullition and porewater samples from pond Types 1 and 2 are comparable to the mean signature of diffusive CH_4 flux (-79.6 ± 0.6‰) documented from a partly thawed *Sphagnum spp*. ombrotrophic bog at Stordalen Mire (McCalley et al., 2014). Type 3 ponds are surrounded by collapsing and remnant palsas and are some of the deepest ponds in this study with significantly higher daily ebullitive CH_4 flux than all other pond types (Burke et al., 2019). The transitional isotopic composition of Type 3 may be indicative of a transitional thaw stage as well from partly or fully thawed bog-like environment to a fully thawed fen-like environment. Type 4 ponds have open water and are hydrologically connected and experience input from adjacent fen areas (Burke et al., 2019). The mean $\delta^{13}C\text{-}CH_4$ of ebullition and porewater from Type 4 ponds is comparable to the mean signature of diffusive CH_4 flux (-66.3 ± 1.6‰) from a fully thawed

E*riophiorum spp.* fen at Stordalen Mire (McCalley et al., 2014). The fully thawed fen had an increased abundance of acetoclastic genus *Methanosaeta* of methanogens (McCalley et al., 2014). Apparent fractionation factor (α_C) was determined by McCalley et al. (2014) to be lower in the *Eriophorum spp*. dominated fen (1.046 ± 0.001) than in the Sphagnum bog (1.053 ± 0.002). Mean α_C follows a comparable trend in this study between pond types, increasing from 1.067 ± 0.0072 in Type 4 to 1.073 ± 0.0057 in Type 1 (Table 1). Permafrost thaw at Stordalen Mire has progressed as permafrost palsa sites transition to ombrotrophic bogs and finally to minerotrophic fens (Johansson et al., 2006; McCalley et al., 2014). Shifts in isotopic composition of ebullitive CH_4 emissions from Types 1 to 4 are comparable to shifts in isotopic composition of diffusive CH_4 emissions as thaw progresses between bogs and fens suggesting that differences between pond types are chronological, with Type 1 being the least thawed and Type 4 being the most thawed, and similar to progressions seen along palsa to fen thaw gradients.

The thaw ponds in this study had dissolved and emitted $\delta^{13}C\text{-}CH_4$ and $\delta D\text{-}CH_4$ values similar to values reported in other thaw pond studies and ebullition measurements from post-glacial lakes also located at Stordalen Mire. Ebullition $\delta D\text{-}CH_4$ values from Types 1-4 were more enriched in δD than data reported from runnel and polygonal ponds in Nunavut, Canada (median -372.9‰; Negandhi et al., 2013) and from alasses in Yakutsk, eastern Siberia (mean -363±20‰; Nakagawa et al., 2002), but were comparable to values from ebullition measurements of neighboring post-glacial lakes located at Stordalen Mire (mean -310.6±21.3‰; Wik et al., 2020). Ebullition $\delta^{13}C\text{-}CH_4$ from Types 1, 2, and 3 in this study were also similar to ebullition $\delta^{13}C\text{-}CH_4$ values measured from these same lakes (mean -67.8±4.6‰; Wik et al., 2020), while Type 4 ebullition was similar to values measured from other thaw ponds in Canada (median -58.8‰; Negandhi et al., 2013) and eastern Siberia (mean -61.1±4.4‰; Nakagawa et al., 2002). Dissolved

$\delta^{13}C\text{-}CH_4$ from pond types 1-4 was similar to data measured by Knoblauch et al. (2015) from polygonal ponds in northeast Siberia. Thaw ponds from varying locations have different emitted isotopic composition of CH_4, highlighting the need to better constrain the isotopic emissions from these features to inform the global CH_4 budget.

As increased temperatures cause an increase in permafrost thaw and active layer deepening, thaw pond formation will continue, and existing early stage ponds may transition to later pond types (Type 4). The difference in relative contribution of CH_4 production pathways between pond types suggests that this transition will be accompanied by a general shift from higher relative contribution of HM towards AM dominance in ponds. Northern wetlands have been associated with a narrow range of $\delta^{13}C\text{-}CH_4$ values (-71±1‰) by Fisher et al (2017). The wide range of $\delta^{13}C\text{-}CH_4$ emitted from the ponds in this study counters this and suggests that this range could be an inaccurate representation as larger amounts of emissions come from pond types with relatively enriched $\delta^{13}C\text{-}CH_4$. Top-down models of high latitude CH_4 emissions currently do not account for a shift in $\delta^{13}C\text{-}CH_4$ as thaw progresses and need to incorporate transitioning landscape features including the pond types examined in this study (Deng et al., 2014; McCalley et al., 2014).

IV. 3. TEMPORAL VARIATION IN ISOTOPIC COMPOSITION OF CH_4

Our multi-year dataset of isotopic composition of emitted and dissolved CH_4 remains relatively constant across years with limited shifts in $\delta^{13}C\text{-}CH_4$ and $\delta D\text{-}CH_4$, supporting our hypothesis that we would not see changes in contribution of methanogenesis pathway within the timeframe of this study (Figure 5c, 5d, 7c, 7d). Despite general stability in contribution of production pathways, we do see that ebullition $\delta^{13}C\text{-}CH_4$ and porewater $\delta D\text{-}CH_4$ become significantly more depleted over the duration respective sampling periods (Figure 5d, 7c). There

is a lack of literature studying dissolved and emitted CH_4 from thaw-formed ponds for extended periods of time (>3 years; Blodau et al., 2008; Knoblauch et al., 2015; Nakagawa et al., 2002; Negandhi et al., 2013) so it is difficult to determine what could be driving the depletion of stable isotopes of CH_4. Based on previous work conducted in bog and fen areas if thaw is driving a transition between pond types towards conditions more similar to Types 3 and 4 we could expect to see a directional shift towards more enriched $\delta^{13}C$ as is seen in transitions from relatively depleted $\delta^{13}C$ to relatively enriched along bog to fen thaw gradients (McCalley et al., 2014). Progression of thaw to more fen-like Type 4 ponds could also explain the depletion in $\delta D\text{-}CH_4$ from 2017 to 2019 (Figure 7c). However, it is unlikely that this shift is happening over a three or even seven year time frame given that permafrost thaw and subsequent vegetation shifts occur on a decadal scale at Stordalen Mire (Johansson et al., 2006). Alternatively, the depletion of ebullition $\delta^{13}C\text{-}CH_4$ between years could indicate a sampling bias, specifically in the ebullition $\delta^{13}C\text{-}CH_4$ data which has the largest number of samples in 2019 relative to all other years (Table 1; Figure 5d). More enriched $\delta^{13}C\text{-}CH_4$ in sampling years prior to 2019 could be due to a larger number of samples collected from Types 3 and 4 with more enriched signatures. If the ponds in this study continue to be monitored to examine long-term variation in isotopic composition of CH_4 ebullition is will be critical to maintain even sample distribution across pond types.

Non-directional significant differences are seen in $\delta^{13}C$ of dissolved CH_4 that may be explained by climatic differences between sampling years (Figure 5c). In permafrost wetlands, increases in precipitation can cause narrowing of the range of values for $\delta^{13}C$ and δD of dissolved CH_4 (Shingubara et al., 2019). Differences in precipitation could be driving the significant enrichment of porewater $\delta^{13}C\text{-}CH_4$ in 2016 relative to other years.

On a monthly timescale, there were no significant differences in $\delta D\text{-}CH_4$ from ebullition or porewater samples between months during the time period from 2017 to 2019 (Figure 7a, 7b), further supporting our hypothesis that there would be no difference in isotopic composition of CH_4 between sampling months. There were however significant differences in $\delta^{13}C\text{-}CH_4$ between months (Figure 5a, 5b). The depletion of porewater $\delta^{13}C\text{-}CH_4$ from June to August may be due to the low sample count in September rather than a reflection of CH_4 production mechanisms, as $\delta^{13}C\text{-}CH_4$ is not significantly different from June to August when sample counts are more evenly distributed (Figure 5a). Ebullition $\delta^{13}C\text{-}CH_4$ becomes significantly more enriched from June to August, contrary to previous findings that $\delta^{13}C\text{-}CH_4$ of ebullition does not change significantly on a seasonal timescale (Jansen et al., 2019; Wik et al., 2020). When porewater and ebullition $\delta^{13}C\text{-}CH_4$ was grouped by pond it became evident that significant differences between months are driven by Pond F only (Table 7, 9, S2, S4) and are not representative of all ponds in this study. Pond F is Type 3 which we believe to be a transitional pond type. The shifts in monthly isotopic composition could be driven by active layer deepening around this pond as temperatures increase over the duration of the growing season, causing an influx of decomposed organic matter from the surrounding collapsing permafrost. This could be determined by collecting further data on the quality of carbon available in Pond F and other ponds in the study during the growing season. Individual conditions that could be driving shifts in $\delta^{13}C\text{-}CH_4$ within this particular pond over the duration of the sampling season need to be further investigated.

V. SUMMARY AND CONCLUDING STATEMENTS

We measured the isotopic composition of $\delta^{13}C\text{-}CH_4$, $\delta D\text{-}CH_4$, and $\delta^{13}C\text{-}CO_2$ from porewater and ebullitive flux of nine thaw ponds categorized into four types (Burke et al., 2019)

over a seven year period and determined that relative contribution of hydrogenotrophic and acetoclastic methanogenesis pathways. Mean $\delta^{13}C\text{-}CH_4$ of each pond type fell within hypothesized ranges for higher relative contribution of HM versus AM, but $\delta D\text{-}CH_4$ was not clearly associated with production effects with the exception of Type 4. This may be a result of depleted $\delta D\text{-}H_2O$ occurring in northern terrestrial ecosystems, making production effects difficult to interpret from $\delta D\text{-}CH_4$. The apparent fractionation factor was key to identifying differences in dominant production pathway between pond types because it helps to further identify CH_4 production effects. Comparison to bog and fen sites at Stordalen Mire indicate that Type 1, 2 ponds are most comparable to bogs in their isotopic composition of CH_4 and have higher relative contributions of HM, Type 3 is also comparable to bog sites but with values that suggest a more even mix of contribution of HM and AM relative to Types 1 and 2. The Type 4 $\delta^{13}C\text{-}CH_4$ and $\delta D\text{-}CH_4$ isotopic signatures indicate higher relative contribution of AM than in the other pond types. The shift in isotopic composition of CH_4 moving from pond type 1 to 4 is similar to thaw progressions from bog to fen documented at Stordalen Mire, suggesting that pond types are representative of thaw stages. Increased warming and permafrost thaw in northern permafrost peatlands has the potential to shift the relative contribution of methanogenesis pathways in these systems from higher contribution of HM to AM, and the overall $\delta^{13}C\text{-}CH_4$ signatures of landscapes. However, this transition between pond types has not been documented within the timeframe of this study. This work highlights the need for accurate determination of the isotopic composition of thaw pond systems to constrain the global CH_4 budget that does not currently account for the relatively enriched $\delta^{13}C\text{-}CH_4$ from northern wetlands.

LIST OF REFERENCES

Anthony, K. M. W., Lindgren, P., Hanke, P., Engram, M., Anthony, P., Daanen, R., Bondurant, A. C., Liljedahl, A. K., Lenz, J., Grosse, G., Jones, B. M., Brosius, L., James, S. R., Minsley, B. J., Pastick, N. J., Munk, J., Chanton, J., Miller, C. E., & Meyer, F. J. (2020). Decadal-scale hotspot methane ebullition within lakes following abrupt permafrost thaw. *Environmental Research Letters*. https://doi.org/10.1088/1748-9326/abc848

Bastviken, D., Tranvik, L. J., Downing, J. A., Crill, P. M., & Enrich-Prast, A. (2011). Freshwater Methane Emissions Offset the Continental Carbon Sink. *Science*, *331*(6013), 50–50. https://doi.org/10.1126/science.1196808

Bellisario, L. M., Bubier, J. L., Moore, T. R., & Chanton, J. P. (1999). Controls on CH_4 emissions from a northern peatland. *Global Biogeochemical Cycles*, *13*(1), 81–91. https://doi.org/10.1029/1998GB900021

Berger, S., Praetzel, L. S. E., Goebel, M., Blodau, C., & Knorr, K.-H. (2018). Differential response of carbon cycling to long-term nutrient input and altered hydrological conditions in a continental Canadian peatland. *Biogeosciences*, *15*(3), 885–903. https://doi.org/10.5194/bg-15-885-2018

Blodau, C., Rees, R., Flessa, H., Rodionov, A., Guggenberger, G., Knorr, K.-H., Shibistova, O., Zrazhevskaya, G., Mikheeva, N., & Kasansky, O. A. (2008). A snapshot of CO2 and CH4 evolution in a thermokarst pond near Igarka, northern Siberia. *Journal of Geophysical Research: Biogeosciences*, *113*(G3). https://doi.org/10.1029/2007JG000652

Burke, S. A., Wik, M., Lang, A., Contosta, A. R., Palace, M., Crill, P. M., & Varner, R. K. (2019). Long-Term Measurements of Methane Ebullition From Thaw Ponds. *Journal of Geophysical Research: Biogeosciences*, *124*(7), 2208–2221. https://doi.org/10.1029/2018JG004786

Callaghan, T. V., Bergholm, F., Christensen, T. R., Jonasson, C., Kokfelt, U., & Johansson, M. (2010). A new climate era in the sub-Arctic: Accelerating climate changes and multiple impacts. *Geophysical Research Letters*, *37*(14). https://doi.org/10.1029/2009GL042064

Chanton, J. P. (2005). The effect of gas transport on the isotope signature of methane in wetlands. *Organic Geochemistry*, *36*(5), 753–768. https://doi.org/10.1016/j.orggeochem.2004.10.007

Chanton, J. P., Fields, D., & Hines, M. E. (2006). Controls on the hydrogen isotopic composition of biogenic methane from high-latitude terrestrial wetlands. *Journal of Geophysical Research: Biogeosciences*, *111*(G4). https://doi.org/10.1029/2005JG000134

Chanton, J. P., & Martens, C. S. (1988). Seasonal variations in ebullitive flux and carbon isotopic composition of methane in a tidal freshwater estuary. *Global Biogeochemical Cycles*, *2*(3), 289–298. https://doi.org/10.1029/GB002i003p00289

Conrad, R. (2005). Quantification of methanogenic pathways using stable carbon isotopic signatures: A review and a proposal. *Organic Geochemistry*, *36*(5), 739–752. https://doi.org/10.1016/j.orggeochem.2004.09.006

Corbett, J., Tfaily, M., Burdige, D., Cooper, W., Glaser, P., & Chanton, J. (2013). Partitioning pathways of CO production in peatlands with stable carbon isotopes. *Biogeochemistry*, *114*(1–3), 327–340. https://doi.org/10.1007/s10533-012-9813-1

Deng, J., Li, C., Frolking, S., Zhang, Y., Bäckstrand, K., & Crill, P. (2014). Assessing effects of permafrost thaw on C fluxes based on multiyear modeling across a permafrost thaw gradient at Stordalen, Sweden. *Biogeosciences*, *11*(17), 4753–4770. https://doi.org/10.5194/bg-11-4753-2014

Flanagan, L. B., Ehleringer, J. R., & Pataki, D. E. (2004). *Stable Isotopes and Biosphere - Atmosphere Interactions: Processes and Biological Controls*. Elsevier.

Greenup, A. L., Bradford, M. A., McNamara, N. P., Ineson, P., & Lee, J. A. (2000). *The role of Eriophorum vaginatum in CH4 flux from an ombrotrophic peatland*. 8.

Holmes, C. D., Prather, M. J., Søvde, O. A., & Myhre, G. (2013). Future methane, hydroxyl, and their uncertainties: Key climate and emission parameters for future predictions. *Atmospheric Chemistry and Physics*, *13*(1), 285–302. https://doi.org/10.5194/acp-13-285-2013

Hornibrook, E. R. C., Longstaffe, F. J., & Fyfe, W. S. (1997). Spatial distribution of microbial methane production pathways in temperate zone wetland soils: Stable carbon and hydrogen isotope evidence. *Geochimica et Cosmochimica Acta*, *61*(4), 745–753. https://doi.org/10.1016/S0016-7037(96)00368-7

Jansen, J., Thornton, B. F., Jammet, M. M., Wik, M., Cortés, A., Friborg, T., MacIntyre, S., & Crill, P. M. (2019). Climate-Sensitive Controls on Large Spring Emissions of CH_4 and CO_2 From Northern Lakes. *Journal of Geophysical Research: Biogeosciences*, *124*(7), 2379–2399. https://doi.org/10.1029/2019JG005094

Johansson, T., Malmer, N., Crill, P. M., Friborg, T., Åkerman, J. H., Mastepanov, M., & Christensen, T. R. (2006). Decadal vegetation changes in a northern peatland, greenhouse gas fluxes and net radiative forcing. *Global Change Biology*, *12*(12), 2352–2369. https://doi.org/10.1111/j.1365-2486.2006.01267.x

Johnston, C. E., Ewing, S. A., Harden, J. W., Varner, R. K., Wickland, K. P., Koch, J. C., Fuller, C. C., Manies, K., & Jorgenson, M. T. (2014). Effect of permafrost thaw on CO_2 and CH_4 exchange in a western Alaska peatland chronosequence. *Environmental Research Letters*, *9*(8), 085004. https://doi.org/10.1088/1748-9326/9/8/085004

Knoblauch, C., Spott, O., Evgrafova, S., Kutzbach, L., & Pfeiffer, E.-M. (2015). Regulation of methane production, oxidation, and emission by vascular plants and bryophytes in ponds of the northeast Siberian polygonal tundra. *Journal of Geophysical Research: Biogeosciences*, *120*(12), 2525–2541. https://doi.org/10.1002/2015JG003053

Kuhn, M., Lundin, E. J., Giesler, R., Johansson, M., & Karlsson, J. (2018). Emissions from thaw ponds largely offset the carbon sink of northern permafrost wetlands. *Scientific Reports*, *8*(1), 9535. https://doi.org/10.1038/s41598-018-27770-x

McCalley, C. K., Woodcroft, B. J., Hodgkins, S. B., Wehr, R. A., Kim, E.-H., Mondav, R., Crill, P. M., Chanton, J. P., Rich, V. I., Tyson, G. W., & Saleska, S. R. (2014). Methane dynamics regulated by microbial community response to permafrost thaw. *Nature*, *514*(7523), 478–481. https://doi.org/10.1038/nature13798

Nakagawa, F., Yoshida, N., Nojiri, Y., & Makarov, V. (2002). Production of methane from alasses in eastern Siberia: Implications from its 14C and stable isotopic compositions. *Global Biogeochemical Cycles*, *16*(3), 14-1-14–15. https://doi.org/10.1029/2000GB001384

Negandhi, K., Laurion, I., Whiticar, M. J., Galand, P. E., Xu, X., & Lovejoy, C. (2013). Small Thaw Ponds: An Unaccounted Source of Methane in the Canadian High Arctic. *PLoS ONE*, *8*(11), e78204. https://doi.org/10.1371/journal.pone.0078204

Noyce, G. L., Varner, R. K., Bubier, J. L., & Frolking, S. (2014). Effect of Carex rostrata on seasonal and interannual variability in peatland methane emissions. *Journal of Geophysical Research: Biogeosciences*, *119*(1), 24–34. https://doi.org/10.1002/2013JG002474

Olsen, M. S., Callaghan, T. V., Reist, J. D., Reiersen, L. O., Dahl-Jensen, D., Granskog, M. A., Goodison, B., Hovelsrud, G. K., Johansson, M., Kallenborn, R., Key, J., Klepikov, A., Meier, W., Overland, J. E., Prowse, T. D., Sharp, M., Vincent, W. F., & Walsh, J. (2011). The Changing Arctic Cryosphere and Likely Consequences: An Overview. *AMBIO*, *40*(S1), 111–118. https://doi.org/10.1007/s13280-011-0220-y

Palace, M., Herrick, C., DelGreco, J., Finnell, D., Garnello, A., McCalley, C., McArthur, K., Sullivan, F., & Varner, R. (2018). Determining Subarctic Peatland Vegetation Using an Unmanned Aerial System (UAS). *Remote Sensing*, *10*(9), 1498. https://doi.org/10.3390/rs10091498

Prater, J. L., Chanton, J. P., & Whiting, G. J. (2007). Variation in methane production pathways associated with permafrost decomposition in collapse scar bogs of Alberta, Canada: VARIATION IN METHANE PRODUCTION. *Global Biogeochemical Cycles*, *21*(4), n/a-n/a. https://doi.org/10.1029/2006GB002866

Quinton, W. L., Hayashi, M., & Chasmer, L. E. (2011). Permafrost-thaw-induced land-cover change in the Canadian subarctic: Implications for water resources. *Hydrological Processes*, *25*(1), 152–158. https://doi.org/10.1002/hyp.7894

Saunois, M., Stavert, A. R., Poulter, B., Bousquet, P., Canadell, J. G., Jackson, R. B., Raymond, P. A., Dlugokencky, E. J., Houweling, S., Patra, P. K., Ciais, P., Arora, V. K., Bastviken, D., Bergamaschi, P., Blake, D. R., Brailsford, G., Bruhwiler, L., Carlson, K. M., Carrol, M., … Zhuang, Q. (2020). The Global Methane Budget 2000–2017. *Earth System Science Data*, *12*(3), 1561–1623. https://doi.org/10.5194/essd-12-1561-2020

Schuur, E. A. G., McGuire, A. D., Schädel, C., Grosse, G., Harden, J. W., Hayes, D. J., Hugelius, G., Koven, C. D., Kuhry, P., Lawrence, D. M., Natali, S. M., Olefeldt, D., Romanovsky, V. E., Schaefer, K., Turetsky, M. R., Treat, C. C., & Vonk, J. E. (2015). Climate change and the permafrost carbon feedback. *Nature*, *520*(7546), 171–179. https://doi.org/10.1038/nature14338

Shingubara, R., Sugimoto, A., Murase, J., Iwahana, G., Tei, S., Liang, M., Takano, S., Morozumi, T., & Maximov, T. C. (2019). Multi-year effect of wetting on CH₄ flux at taiga–tundra boundary in northeastern Siberia deduced from stable isotope ratios of CH₄ *Biogeosciences*, *16*(3), 755–768. https://doi.org/10.5194/bg-16-755-2019

Svensson, B. H., Christensen, T. R., Johansson, E., & Oquist, M. (1999). Interdecadal Changes in CO 2 and CH 4 Fluxes of a Subarctic Mire: Stordalen Revisited after 20 Years. *Oikos*, *85*(1), 22. https://doi.org/10.2307/3546788

Townsend-Small, A., Åkerström, F., Arp, C. D., & Hinkel, K. M. (2017). Spatial and Temporal Variation in Methane Concentrations, Fluxes, and Sources in Lakes in Arctic Alaska. *Journal of Geophysical Research: Biogeosciences*, *122*(11), 2966–2981. https://doi.org/10.1002/2017JG004002

Turetsky, M. R., Abbott, B. W., Jones, M. C., Walter Anthony, K., Olefeldt, D., Schuur, E. A. G., Koven, C., McGuire, A. D., Grosse, G., Kuhry, P., Hugelius, G., Lawrence, D. M., Gibson, C., & Sannel, A. B. K. (2019). Permafrost collapse is accelerating carbon release. *Nature*, *569*(7754), 32–34. https://doi.org/10.1038/d41586-019-01313-4

Vitt, D. H., Halsey, L. A., & Zoltai, S. C. (2000). *The changing landscape of Canada's western boreal forest: The current dynamics of permafrost*. *30*, 5.

Waldron, S., Lansdown, J. M., Scott, E. M., Fallick, A. E., & Hall, A. J. (1999). The global influence of the hydrogen isotope composition of water on that of bacteriogenic methane from shallow freshwater environments. *Geochimica et Cosmochimica Acta*, *63*(15), 2237–2245. https://doi.org/10.1016/S0016-7037(99)00192-1

Walter, K. M., Smith, L. C., & Chapin, F. S. (2007). Methane Bubbling from Northern Lakes: Present and Future Contributions to the Global Methane Budget. *Philosophical Transactions: Mathematical, Physical and Engineering Sciences*, *365*(1856), 1657–1676.

Whiticar, Michael J. (1999). Carbon and hydrogen isotope systematics of bacterial formation and oxidation of methane. *Chemical Geology*, *161*(1–3), 291–314. https://doi.org/10.1016/S0009-2541(99)00092-3

Whiticar, M.J, Faber, E., & Schoell, M. (1986). Biogenic methane formation in marine and freshwater environments: CO2 reduction vs. acetate fermentation—Isotope evidence. *Geochimica et Cosmochimica Acta*, *50*(5), 693–709. https://doi.org/10.1016/0016-7037(86)90346-7

Wik, M., Crill, P. M., Varner, R. K., & Bastviken, D. (2013). Multiyear measurements of ebullitive methane flux from three subarctic lakes: METHANE EBULLITION FROM SUBARCTIC LAKES. *Journal of Geophysical Research: Biogeosciences*, *118*(3), 1307–1321. https://doi.org/10.1002/jgrg.20103

Wik, M., Thornton, B. F., Varner, R. K., McCalley, C., & Crill, P. M. (2020). Stable methane isotopologues from northern lakes suggest ebullition is dominated by sub-lake scale processes. *Journal of Geophysical Research: Biogeosciences*. https://doi.org/10.1029/2019JG005601

Wik, M., Varner, R. K., Anthony, K. W., MacIntyre, S., & Bastviken, D. (2016). Climate-sensitive northern lakes and ponds are critical components of methane release. *Nature Geoscience*, *9*(2), 99–105. https://doi.org/10.1038/ngeo2578

APPENDIX

APPENDIX A. TEMPORAL PAIRWISE COMPARISONS OF EBULLITION AND POREWATER $\delta^{13}C\text{-}CH_4$ AND $\delta D\text{-}CH_4$ BY POND

Table A1. Pairwise comparisons across sampling years within ponds for ebullition $\delta^{13}C\text{-}CH_4$ data using the Dunn's test following the Bonferroni method ($\alpha = 0.05$). Significant p-values indicated by *. Ponds with NA values had insufficient data for the comparison.

Pairwise comparison of ebullition $\delta^{13}C\text{-}CH_4$ by year					
Pond A		***p***	**Pond E**		***p***
2019	2017	1	2018	2017	0.0451*
2019	2016	0.5458	2019	2017	1
2017	2016	0.4068	2018	2016	1
Pond B		***p***	2019	2016	1
		NA	2019	2018	0.3287
Pond C		***p***	2017	2016	0.1373
2017	2016	1	**Pond F**		***p***
2017	2012	0.981	2018	2017	0.5604
2019	2018	1	2019	2017	1
2019	2016	1	2019	2018	1
2019	2012	1	2018	2016	1
2016	2012	1	2019	2016	0.2218
2018	2016	1	2017	2016	0.0257
2018	2012	1	**Pond G**		***p***
2019	2017	0.8148			*NA*
2018	2017	0.7376	**Pond H**		***p***
Pond D		***p***	2019	2018	1
2017	2016	0.343	2016	2012	1
2019	2016	0.6541	2017	2012	1
2019	2017	1	2017	2016	1
			2019	2017	1
			2019	2012	0.0109*
			2018	2017	0.8831
			2019	2016	0.0469
			2018	2012	0.1291
			2018	2016	0.1079

Table A2. Pairwise comparisons across sampling months within ponds for ebullition $\delta^{13}C\text{-}CH_4$ data using the Dunn's test following the Bonferroni method ($\alpha = 0.05$). Significant p-values indicated by *. Ponds with NA values had insufficient data for the comparison.

Pairwise comparison of ebullition $\delta^{13}C\text{-}CH_4$ by month					
Pond A		**p**	**Pond E**		**p**
August	June	0.7735	August	June	0.0662
August	July	0.3007	July	June	0.3603
July	June	1	August	July	1
Pond B		**p**	**Pond F**		**p**
August	June	0.4247	August	July	0.0425*
July	June	1	August	June	0.6997
August	July	1	July	June	1
Pond C		**p**	**Pond G**		**p**
July	June	1	August	July	0.4469
August	June	1	**Pond H**		**p**
August	July	1	August	June	0.0819
Pond D		**p**	July	June	0.3727
July	June	0.6686	August	July	0.8072
August	June	1	**Pond I**		**p**
August	July	0.3686			*NA*

Table A3. Pairwise comparisons across sampling years within ponds for porewater $\delta^{13}C\text{-}CH_4$ data using the Tukey-Kramer HSD test. Significant p-values indicated by *. Ponds with NA values had insufficient data for the comparison.

Pairwise comparison of porewater $\delta^{13}C\text{-}CH_4$ by year					
Pond A		***p***	**Pond E**		***p***
2016	2018	<.0001*	2016	2017	<.0001*
2014	2018	<.0001*	2016	2018	<.0001*
2016	2017	0.0013*	2014	2017	0.0074*
2016	2019	0.0038*	2016	2019	0.0006*
2019	2018	0.0154*	2014	2018	0.0314*
2017	2018	0.1614	2014	2019	0.4171
2014	2017	0.0868	2019	2017	0.1229
2016	2014	0.1221	2016	2014	0.5523
2014	2019	0.2625	2019	2018	0.4235
2019	2017	0.9544	2018	2017	0.9771

Pond B		***p***
2014	2017	0.4873
2014	2019	0.5175
2018	2017	0.6482
2018	2019	0.6765
2014	2018	0.9987
2019	2017	0.9999
Pond C		***p***
2016	2014	0.0181*
2016	2018	0.2074
2017	2014	0.2247
2016	2019	0.4487
2019	2014	0.5378
2016	2017	0.6937
2017	2018	0.8592
2018	2014	0.8238
2019	2018	0.9885
2017	2019	0.9892
Pond D		***p***
2017	2018	0.0376*
2014	2018	0.0862
2016	2018	0.0856
2017	2019	0.1722
2014	2019	0.3814
2016	2019	0.3861
2019	2018	0.7583
2017	2016	0.9501
2017	2014	0.9673
2014	2016	1

Pond F		***p***
2016	2018	<.0001*
2016	2014	<.0001*
2016	2017	0.0009*
2019	2018	0.0107*
2019	2014	0.0288*
2016	2019	0.0674
2017	2018	0.2926
2019	2017	0.4973
2017	2014	0.5111
2014	2018	0.9957
Pond G		***p***
		NA
Pond H		***p***
2018	2019	0.5435
2018	2016	0.7924
2016	2019	0.8116
Pond I		***p***
		NA

Table A4. Pairwise comparisons across sampling months within ponds for porewater $\delta^{13}C\text{-}CH_4$ data using the Tukey-Kramer HSD test. Significant p-values indicated by *. Ponds with NA values had insufficient data for the comparison.

Pairwise comparison of porewater $\delta^{13}C\text{-}CH_4$ by month					
Pond A		***p***	**Pond E**		***p***
June	August	0.1088	September	July	0.8701
June	July	0.129	June	July	0.3048
September	August	0.6246	August	July	0.5387
September	July	0.7791	September	August	0.9845
June	September	0.8991	September	June	0.9917
July	August	0.9449	June	August	0.9961
Pond B		***p***	**Pond F**		***p***
September	July	0.1514	June	September	0.543
September	June	0.4076	June	August	0.0176*
September	August	0.5581	July	September	0.8478
August	July	0.6966	July	August	0.2003
June	July	0.8459	June	July	0.3603
August	June	0.9904	August	September	1
Pond C		***p***	**Pond G**		***p***
June	September	0.1495	**NA**		
June	August	0.181	**Pond H**		***p***
June	July	0.1867	June	July	0.7035
July	September	0.6587	August	July	0.8521
August	September	0.707	June	August	0.8766
July	August	0.999	**Pond I**		***p***
Pond D		***p***	August	September	0.7241
June	July	0.3528			
August	July	0.5517			
June	September	0.9217			
August	September	0.965			
September	July	0.987			
June	August	0.9939			

APPENDIX B. 2019 DAILY BUBBLE FLUX BY POND

I. EBULLITON SAMPLING AND ANALYSIS

Ebullition (bubble) samples were collected from the seven study ponds during the growing season (June - August) in 2019; No samples were collected in 2013 and 2015. Every 1-3 days samples were collected from floating bubble traps to assess isotopic composition and calculate daily ebullitive flux (Figure 2). Bubble traps were deployed using methodology described in detail by Burke et al. (2019) and were designed similarly to bubble traps used by Wik et al. (2013). Ebullitive flux samples were processed as described by Burke et al. (2019). In summary, the accumulated gas was store in 10-ml polypropylene syringes and refrigerated at 2°C for up to 48hours prior to analysis with a gas chromatograph-flame ionization detector (GC-FID) at the Abisko Scientific Research Station (ANS).

II. FLUX RESULTS BY POND

Table A5. Sample count, range and average daily bubble flux for seven ponds in this study from the 2019 sampling season. Daily bubble flux varied widely between the ponds surveyed but were highest from Type 3 ponds E and F, consistent with previous findings from Burke et al. (2019).

Pond	Pond type from Burke et al. (2019)	Minimum flux (mg CH_4 $m^{-2}d^{-1}$)	Median flux (mg CH_4 $m^{-2}d^{-1}$)	Maximum flux (mg CH_4 $m^{-2}d^{-1}$)	Mean flux (mg CH_4 $m^{-2}d^{-1}$)	Sample count
A	1	0.0	0.1	56.6	7.6 ± 18.2	22
B	1	0.1	0.1	2.7	0.4 ± 0.6	30
C	2	0.0	0.7	463.9	28.6 ± 95.8	24
D	2	0.0	0.3	6.8	0.7 ± 1.5	19
E	3	0.0	41.0	432.5	69.1 ± 81.9	81
F	3	0.3	79.6	2001.7	131.5 ± 234.0	88
H	4	0.0	14.1	96.7	27.6 ± 27.4	40

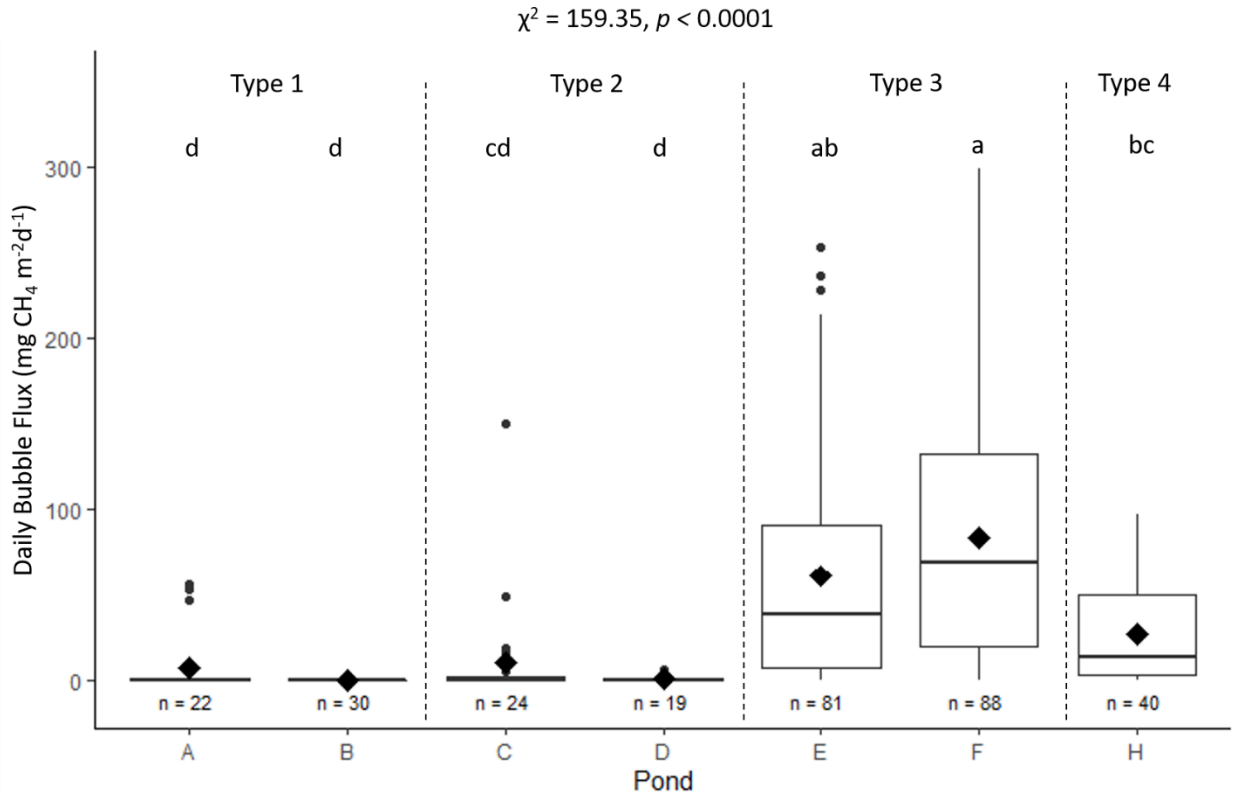

Figure A1. Daily bubble flux (mg CH_4 $m^{-2}d^{-1}$) from seven ponds included in this study during the 2019 sampling season. The y-axis was plotted between 0 and 350 mg CH_4 $m^{-2}d^{-1}$ to better display the distribution of the data. Outliers greater than 350 mg CH_4 $m^{-2}d^{-1}$ are omitted from this figure. Whiskers represent the 10th and 90th percentiles and black dots represent outliers. Black diamonds and horizontal black lines across boxes denote means and medians respectively. The number of samples (*n*) in each group is noted along the bottom. Daily bubble flux data was not normally distributed ($p < 0.0001$, Anderson-Darling test for normality) and was assessed using the Kruskal-Wallis rank sum test, results of which are noted as χ^2 and *p*. Lowercase letters indicate pairwise differences between ponds as determined by a Dunn's test following the Bonferroni method ($\alpha = 0.05$). Daily bubble flux varied widely but was significantly different between individual ponds. The pond type associated with each pond by Burke et al. (2019) is noted along the top of the figure.